









# TECH BRIEFS

NATIONAL AERONAUTICS AND SPACE ADMINISTRATION

-  **Technology Focus**
-  **Computers/Electronics**
-  **Software**
-  **Materials**
-  **Mechanics**
-  **Machinery/Automation**
-  **Manufacturing**
-  **Bio-Medical**
-  **Physical Sciences**
-  **Information Sciences**
-  **Books and Reports**



# INTRODUCTION

Tech Briefs are short announcements of innovations originating from research and development activities of the National Aeronautics and Space Administration. They emphasize information considered likely to be transferable across industrial, regional, or disciplinary lines and are issued to encourage commercial application.

## Availability of NASA Tech Briefs and TSPs

Requests for individual Tech Briefs or for Technical Support Packages (TSPs) announced herein should be addressed to

### National Technology Transfer Center

Telephone No. (800) 678-6882 or via World Wide Web at [www2.nttc.edu/leads/](http://www2.nttc.edu/leads/)

Please reference the control numbers appearing at the end of each Tech Brief. Information on NASA's Commercial Technology Team, its documents, and services is also available at the same facility or on the World Wide Web at [www.nctn.hq.nasa.gov](http://www.nctn.hq.nasa.gov).

Commercial Technology Offices and Patent Counsels are located at NASA field centers to provide technology-transfer access to industrial users. Inquiries can be made by contacting NASA field centers and program offices listed below.

## NASA Field Centers and Program Offices

### Ames Research Center

Lisa L. Lockyer  
(650) 604-3009  
[lisa.l.lockyer@nasa.gov](mailto:lisa.l.lockyer@nasa.gov)

### Dryden Flight Research Center

Gregory Poteat  
(661) 276-3872  
[greg.poteat@dfrc.nasa.gov](mailto:greg.poteat@dfrc.nasa.gov)

### Goddard Space Flight Center

Nona Cheeks  
(301) 286-5810  
[Nona.K.Cheeks.1@gsfc.nasa.gov](mailto:Nona.K.Cheeks.1@gsfc.nasa.gov)

### Jet Propulsion Laboratory

Ken Wolfenbarger  
(818) 354-3821  
[james.k.wolfenbarger@jpl.nasa.gov](mailto:james.k.wolfenbarger@jpl.nasa.gov)

### Johnson Space Center

Charlene E. Gilbert  
(281) 483-3809  
[commercialization@jsc.nasa.gov](mailto:commercialization@jsc.nasa.gov)

### Kennedy Space Center

Jim Aliberti  
(321) 867-6224  
[Jim.Aliberti-1@ksc.nasa.gov](mailto:Jim.Aliberti-1@ksc.nasa.gov)

### Langley Research Center

Jesse Midgett  
(757) 864-3936  
[jesse.c.midgett@nasa.gov](mailto:jesse.c.midgett@nasa.gov)

### John H. Glenn Research Center at Lewis Field

Larry Viterna  
(216) 433-3484  
[cto@grc.nasa.gov](mailto:cto@grc.nasa.gov)

### Marshall Space Flight Center

Vernotto McMillan  
(256) 544-2615  
[vernotto.mcmillan@msfc.nasa.gov](mailto:vernotto.mcmillan@msfc.nasa.gov)

### Stennis Space Center

Robert Bruce  
(228) 688-1929  
[robert.c.bruce@nasa.gov](mailto:robert.c.bruce@nasa.gov)

### NASA Program Offices

At NASA Headquarters there are seven major program offices that develop and oversee technology projects of potential interest to industry:

#### Carl Ray

Small Business Innovation Research Program (SBIR) & Small Business Technology Transfer Program (STTR)  
(202) 358-4652 or  
[cray@nasa.gov](mailto:cray@nasa.gov)

#### Benjamin Neumann

Innovative Technology Transfer Partnerships (Code TD)  
(202) 358-2320  
[benjamin.j.neumann@nasa.gov](mailto:benjamin.j.neumann@nasa.gov)

#### John Mankins

Office of Space Flight (Code TD)  
(202) 358-4659 or  
[john.c.mankins@nasa.gov](mailto:john.c.mankins@nasa.gov)

#### Terry Hertz

Office of Aero-Space Technology (Code RS)  
(202) 358-4636 or  
[thertz@nasa.gov](mailto:thertz@nasa.gov)

#### Glen Mucklow

Office of Space Sciences (Code SM)  
(202) 358-2235 or  
[gmucklow@nasa.gov](mailto:gmucklow@nasa.gov)

#### Roger Crouch

Office of Microgravity Science Applications (Code U)  
(202) 358-0689 or  
[rcrouch@nasa.gov](mailto:rcrouch@nasa.gov)

#### Granville Paules

Office of Mission to Planet Earth (Code Y)  
(202) 358-0706 or  
[gpaules@mtpe.hq.nasa.gov](mailto:gpaules@mtpe.hq.nasa.gov)





# TECH BRIEFS

NATIONAL AERONAUTICS AND SPACE ADMINISTRATION



## 5 Technology Focus: Sensors

- 5 Fiber-Optic Sensor Would Monitor Growth of Polymer Film
- 6 Sensors for Pointing Moving Instruments Toward Each Other
- 6 Pd/CeO<sub>2</sub>/SiC Chemical Sensors
- 6 Microparticle Flow Sensor
- 7 Scattering-Type Surface-Plasmon-Resonance Biosensors
- 8 Diode-Laser-Based Spectrometer for Sensing Gases



## 11 Electronics/Computers

- 11 Improved Cathode Structure for a Direct Methanol Fuel Cell
- 12 X-Band, 17-Watt Solid-State Power Amplifier
- 13 Improved Anode for a Direct Methanol Fuel Cell



## 15 Software

- 15 Tools for Designing and Analyzing Structures
- 15 Interactive Display of Scenes With Annotations
- 15 Solving Common Mathematical Problems
- 15 Tools for Basic Statistical Analysis
- 16 Program Calculates Forces in Bolted Structural Joints
- 16 Integrated Structural Analysis and Test Program



## 17 Materials

- 17 Molybdate Coatings for Protecting Aluminum Against Corrosion
- 18 Synthesizing Diamond From Liquid Feedstock
- 19 Modifying Silicates for Better Dispersion in Nanocomposites



## 21 Machinery/Automation

- 21 Powder-Collection System for Ultrasonic/Sonic Drill/Corer
- 21 Semiautomated, Reproducible Batch Processing of Soy



## 23 Physical Sciences

- 23 Hydrogen Peroxide Enhances Removal of NO<sub>x</sub> From Flue Gases
- 24 Subsurface Ice Probe
- 25 Real-Time Simulation of Aeroheating of the Hyper-X Airplane
- 25 Using Laser-Induced Incandescence To Measure Soot in Exhaust



## 27 Information Sciences

- 27 Method of Real-Time Principal-Component Analysis
- 28 Insect-Inspired Flight Control for Unmanned Aerial Vehicles
- 29 Domain Compilation for Embedded Real-Time Planning
- 30 Semantic Metrics for Analysis of Software
- 30 Simulation of Laser Cooling and Trapping in Engineering Applications



## 33 Books & Reports

- 33 Large Fluvial Fans and Exploration for Hydrocarbons
- 33 Doping-Induced Interband Gain in InAs/AlSb Quantum Wells
- 33 Development of Software for a Lidar-Altitude Processor
- 33 Upgrading the Space Shuttle Caution and Warning System
- 34 Fractal Reference Signals in Pulse-Width Modulation

This document was prepared under the sponsorship of the National Aeronautics and Space Administration. Neither the United States Government nor any person acting on behalf of the United States Government assumes any liability resulting from the use of the information contained in this document, or warrants that such use will be free from privately owned rights.





## Fiber-Optic Sensor Would Monitor Growth of Polymer Film

Changes in thickness would be inferred from interference fringes.

*Goddard Space Flight Center, Greenbelt, Maryland*

A proposed optoelectronic sensor system would measure the increase in thickness of a film of parylene (a thermoplastic polymer made from para-xylylene) during growth of the film in a vapor deposition process. By enabling real-time monitoring of film thickness, the system would make it possible to identify process conditions favorable for growth and to tailor the final thickness of the film with greater precision than is now possible.

The heart of the sensor would be a pair of fiber-optic Fabry-Perot interferometers, depicted schematically in the figure. (In principle, a single such interferometer would suffice. The proposal calls for the use of two interferometers for protective redundancy and increased accuracy.) Each interferometer would include a light source, a fiber-optic coupler, and photodetectors in a control box outside the deposition chamber. A single-mode optical fiber for each interferometer would run from inside the

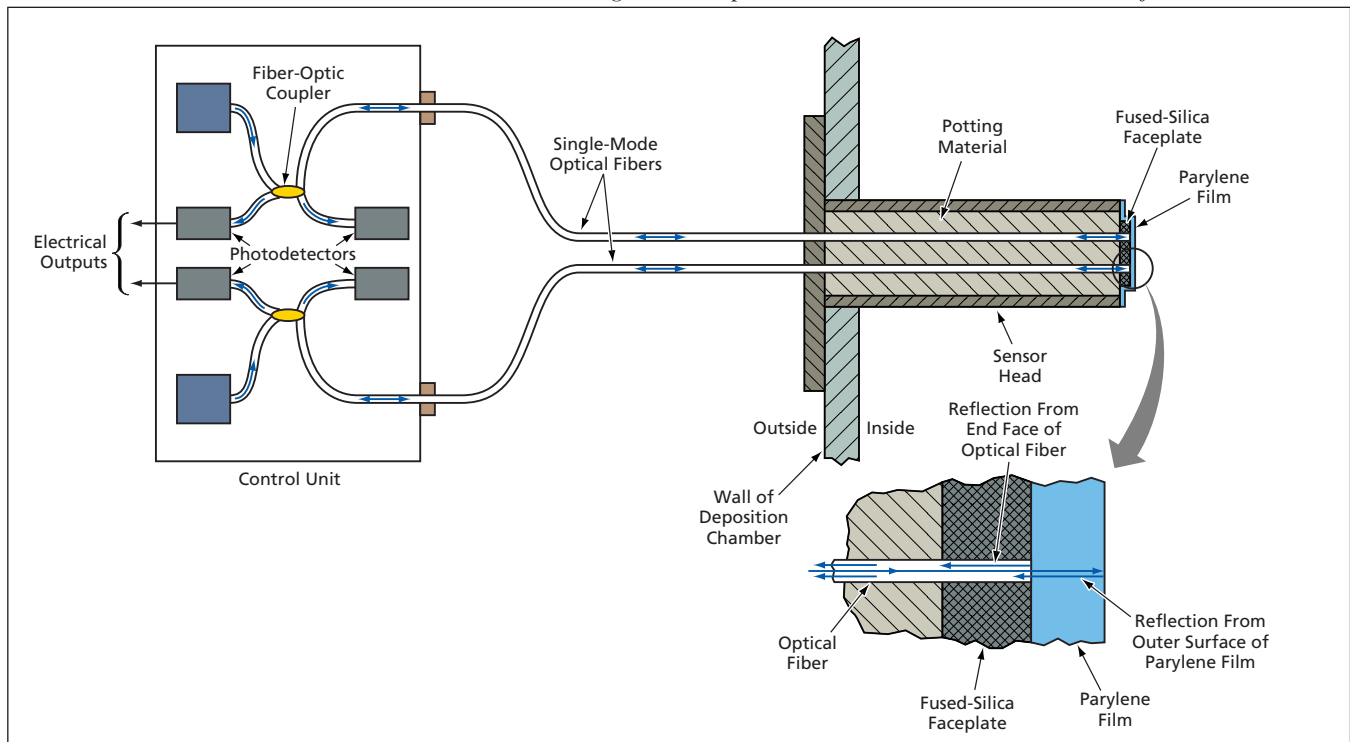
control box to a fused-silica faceplate in a sensor head. The sensory tips of the optical fibers would be polished flush with the free surface of the faceplate. In preparation for use, the sensor head would be mounted with a hermetic seal in a feed-through port in the deposition chamber, such that free face of the faceplate and the sensory tips of the optical fibers would be exposed to the deposition environment.

During operation, light would travel along each optical fiber from the control box to the sensor head. A small portion of the light would be reflected toward the control box from the end face of each fiber. Once growth of the parylene film started, a small portion of the light would also be reflected toward the control box from the outer surface of the film. In the control box, the two reflected portions of the light beam would interfere in one of the photodetectors. The difference between the phases of the interfering reflected portions of the

light beam would vary in proportion to the increasing thickness of the film and the known index of refraction of the film, causing the photodetector reading to vary in proportion to a known sinusoidal function of film thickness. Electronic means of monitoring this variation and the corresponding variation in phase and thickness are well established in the art of interferometry. Hence, by tracking the cumulative change in phase difference from the beginning of deposition, one could track the growing thickness of the film to within a small fraction of a wavelength of light.

*This work was done by Michael Beamesderfer of Goddard Space Flight Center. Further information is contained in a TSP (see page 1).*

*This invention is owned by NASA, and a patent application has been filed. Inquiries concerning nonexclusive or exclusive license for its commercial development should be addressed to the Patent Counsel, Goddard Space Flight Center, (301) 286-7351. Refer to GSC-14757-1.*



Portions of the light beam in each optical fiber would be reflected from opposite faces of the parylene and would interfere in one of the photodetectors. Variations in the photodetector output would be interpreted in terms of increases in the thickness of the parylene film according to well-known principles of interferometry.

---

## Sensors for Pointing Moving Instruments Toward Each Other

*NASA's Jet Propulsion Laboratory, Pasadena, California*

Optoelectronic sensor systems are being developed for use in maintaining fixed relative orientations of two scientific-instrument platforms that are in relative motion. In the original intended application, the platforms would be two spacecraft flying in formation and separated by a long baseline. In principle, sensor systems of this type could also be used in terrestrial applications for maintaining alignments between moving instrument platforms. The sensor system

would utilize beacon laser beams that would be transmitted by the platforms in the normal course of scientific measurements. The frequency of the returned laser beam would differ by about 5 MHz. On each platform, the transmitted laser beam and the laser beam bounced off the other platform would be focused onto a quadrant photodetector, where the interference between the laser beams would give rise to sinusoidal (beat-frequency) signals on all four quadrants. The differ-

ences among the phases of the beat-frequency signals in the quadrants would depend on, and would be used to determine the angle between, the wave fronts of the outgoing and incoming laser beams.

*This work was done by Carl Liebe, Alexander Abramovici, Jacob Chapsky, Daniel Shaddock, Charles Harb, and Frank Dekens of Caltech for NASA's Jet Propulsion Laboratory. Further information is contained in a TSP (see page 1). NPO-40610*

---

## Pd/CeO<sub>2</sub>/SiC Chemical Sensors

**Nanostructured interfacial CeO<sub>2</sub> layers contribute to thermal stability and transfer of electrons.**

*John H. Glenn Research Center, Cleveland, Ohio*

The incorporation of nanostructured interfacial layers of CeO<sub>2</sub> has been proposed to enhance the performances of Pd/SiC Schottky diodes used to sense hydrogen and hydrocarbons at high temperatures. If successful, this development could prove beneficial in numerous applications in which there are requirements to sense hydrogen and hydrocarbons at high temperatures: examples include monitoring of exhaust gases from engines and detecting fires.

Sensitivity and thermal stability are major considerations affecting the development of high-temperature chemical sensors. In the case of a metal/SiC Schottky diode for a number of metals, the SiC becomes more chemically active in the presence of the thin metal film on the SiC surface at high temperature. This increase in chemical reactivity causes changes in chemical composition and structure of the metal/SiC inter-

face. The practical effect of the changes is to alter the electronic and other properties of the device in such a manner as to degrade its performance as a chemical sensor. To delay or prevent these changes, it is necessary to limit operation to a temperature <450 °C for these sensor structures.

The present proposal to incorporate interfacial CeO<sub>2</sub> films is based partly on the observation that nanostructured materials in general have potentially useful electrical properties, including an ability to enhance the transfer of electrons. In particular, nanostructured CeO<sub>2</sub>, that is CeO<sub>2</sub> with nanosized grains, has shown promise for incorporation into high-temperature electronic devices. Nanostructured CeO<sub>2</sub> films can be formed on SiC and have been shown to exhibit high thermal stability on SiC, characterized by the ability to withstand temperatures somewhat greater than 700 °C for lim-

ited times. The exchanges of oxygen between CeO<sub>2</sub> and SiC prevent the formation of carbon and other chemical species that are unfavorable for operation of a SiC-based Schottky diode as a chemical sensor. Consequently, it is anticipated that in a Pd/CeO<sub>2</sub>/SiC Schottky diode, the nanostructured interfacial CeO<sub>2</sub> layer would contribute to thermal stability and, by contributing to transfer of electrons, would also contribute to sensitivity.

*This work was done by Weijie Lu and W. Eugene Collins of Fisk University for Glenn Research Center. Further information is contained in a TSP (see page 1).*

*Inquiries concerning rights for the commercial use of this invention should be addressed to NASA Glenn Research Center, Commercial Technology Office, Attn: Steve Fedor, Mail Stop 4-8, 21000 Brookpark Road, Cleveland, Ohio 44135. Refer to LEW-17332.*

---

## Microparticle Flow Sensor

**As many as 1,000 microparticles can be identified, tracked, and counted.**

*Lyndon B. Johnson Space Center, Houston, Texas*

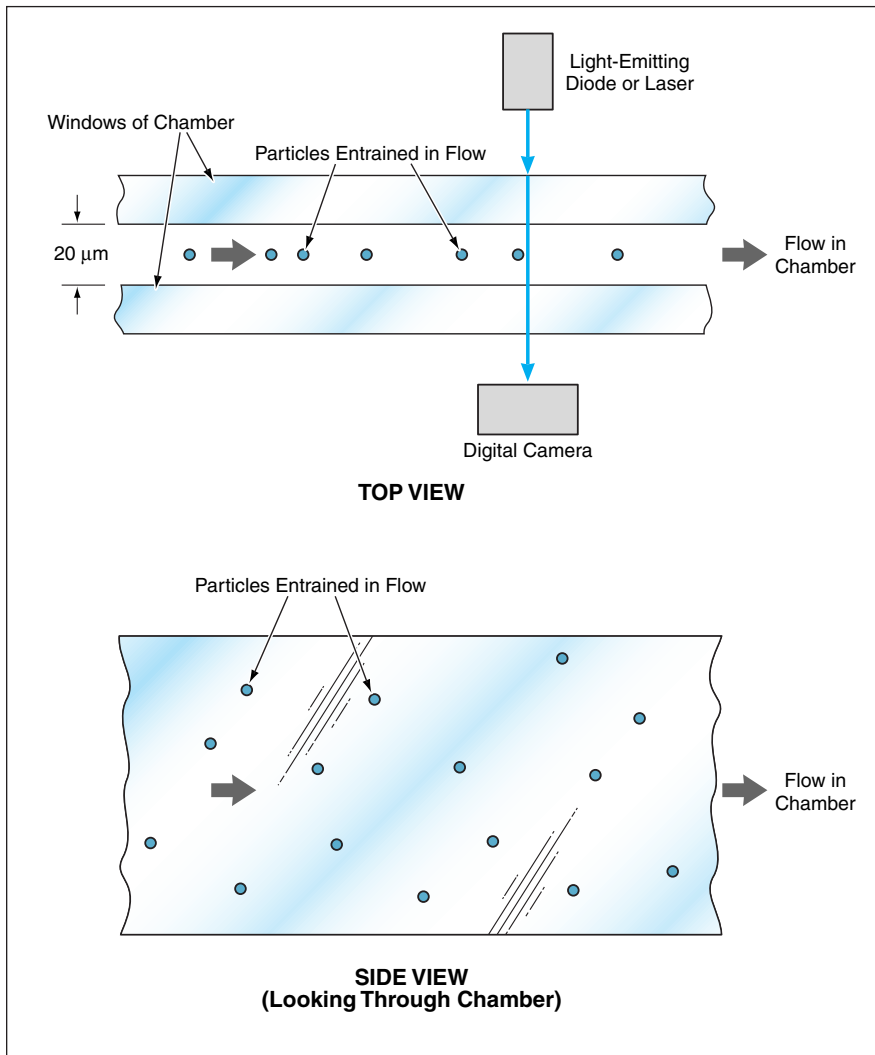
The microparticle flow sensor (MFS) is a system for identifying and counting microscopic particles entrained in a flowing liquid. The MFS includes a transparent, optoelectronically instrumented laminar-flow chamber (see fig-

ure) and a computer for processing instrument-readout data. The MFS could be used to count microparticles (including micro-organisms) in diverse applications — for example, production of microcapsules, treatment of wastewater,

pumping of industrial chemicals, and identification of ownership of liquid products.

In addition to the instrumented chamber and the computer, the system includes a process controller and pumps.





An **Instrumented Laminar-Flow Chamber**, depicted here in greatly simplified form, is designed and operated in a manner that guarantees that microparticles of interest traverse the chamber abreast, so that they can all be illuminated with laser light and monitored by a digital camera.

The instrumentation on the chamber includes one or more laser(s) and/or light-emitting diode(s) for illuminating the microparticles in the flow path, and a high-resolution digital camera with a magnifying lens for capturing sequential

images of the illuminated microparticles as they move across the chamber. The MFS acts partly as a spectrophotometer in that it measures the amount of light reflected or transmitted by each microparticle at the laser wavelength(s).

The chamber is only  $20\ \mu\text{m}$  thick, and the liquid is pumped through it at a rate of about to  $200\ \mu\text{L}/\text{min}$ , giving rise to a low-shear laminar flow that forces the entrained microparticles to move across the chamber abreast. Hence, no microparticle shadows another microparticle, and as a result, every microparticle can be optically observed and analyzed separately from every other microparticle.

Special-purpose software running on a Pentium III 400-MHz computer processes the image data to locate individual microparticles and track their trajectories. If the microparticles of interest have known spectral characteristics (for example, if they have been dyed), then the software can identify the microparticles of interest and/or distinguish them from other microparticles (e.g., sediment) by means of the amounts of light transmitted or reflected by the various microparticles at different wavelengths. Tracking of microparticle trajectories can yield data on sedimentation rates, which are useful for identifying and distinguishing among microparticles of different sizes and compositions. Image data are also analyzed to determine microparticle sizes and shapes, which are also indicative of microparticle identities. The software can count and track more than 1,000 microparticles simultaneously as well as perform statistical analysis of microparticle data. A complete cycle of acquisition and processing of image data is only 5 seconds long.

*This work was done by Dennis R. Morrison of Johnson Space Center.*

*This invention is owned by NASA, and a patent application has been filed. Inquiries concerning nonexclusive or exclusive license for its commercial development should be addressed to the Patent Counsel, Johnson Space Center, (281) 483-0837. Refer to MSC-23277.*

## Scattering-Type Surface-Plasmon-Resonance Biosensors

Sensitivities would greatly exceed those of reflection-type SPR biosensors.

NASA's Jet Propulsion Laboratory, Pasadena, California

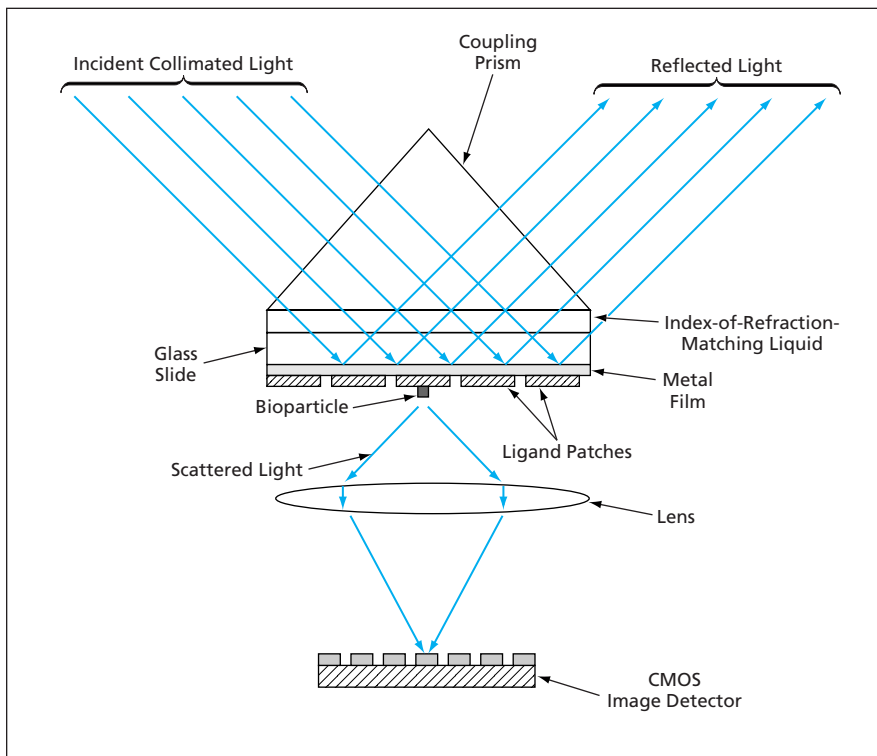
Biosensors of a proposed type would exploit scattering of light by surface plasmon resonance (SPR). Related prior biosensors exploit absorption of light by SPR. Relative to the prior SPR biosensors, the proposed SPR biosensors would offer greater sensitivity — in some cases, enough sensitivity to detect

bioparticles having dimensions as small as nanometers.

A surface plasmon wave can be described as a light-induced collective oscillation in electron density at the interface between a metal and a dielectric. At SPR, most incident photons are either absorbed or scattered at the metal/dielectric

interface and, consequently, reflected light is greatly attenuated. The resonance wavelength and angle of incidence depend upon the permittivities of the metal and dielectric.

An SPR sensor of the type most widely used heretofore includes a gold film coated with a ligand — a substance that



Light Scattered by SPR from a bioparticle/ligand binding site would be focused to a bright spot on an image detector.

binds analyte molecules. The gold film is thin enough to support evanescent-wave coupling through its thickness. The change in the effective index of refraction at the surface, and thus the change in the SPR response, increases with the number of bound analyte molecules. The device is illuminated at a fixed wavelength, and the intensity of light reflected from the gold surface opposite the ligand-coated surface is measured as a function of the angle of incidence. From these measurements, the angle of minimum reflection intensity is determined.

These measurements and the determination of the angle of minimum reflection intensity are performed before and after (and can be performed during) exposure of the sensor to a sample containing the analyte molecules. Any shift in the angle between such succes-

sive determinations is indicative of a change in the concentration of analyte molecules in the sample. This type of sensor is characterized by low sensitivity for the following reasons:

- A small number of analyte molecules gives rise to a small shift in the angle of minimum reflection intensity.
- Because one is measuring a reflection dip rather than a reflection peak, the measurement can be strongly affected by noise. The difficulty of determining the small angular shift is analogous to the difficulty of measuring the shift of a dark spot on a bright background.

A biosensor according to the proposal would afford a much greater signal-to-noise ratio by exploiting SPR in a different way that would involve, literally, a bright spot on a dark background. A proposed sensor (see figure) would include a

coupling prism, an index-of-refraction-matching liquid, a glass slide, and a metal film thin enough to support evanescent-wave coupling. The metal surface to be exposed to the specimen would be coated with ligand in a regular array of patches. The array of patches would be observed by a miniature microscope that would include a lens and a complementary oxide/semiconductor (CMOS) image detector. The microscope would be designed so that each ligand patch would occupy many CMOS pixels and the resolution of the microscope would be close to the optical limit (about one wavelength of the incident light).

The sensor would be illuminated with collimated light at a wavelength and angle of incidence chosen so that SPR would occur whenever and wherever analyte molecules became bound to the ligand. In the absence of such binding, there would be little scattered light. In the presence of such binding at any spot on the ligand, the strong SPR scattering from that spot would cause the spot to be imaged brightly in the microscope. Even a bioparticle smaller than a wavelength of light could induce sufficient SPR scattering to be detectable.

*This work was done by Yu Wang, Bedabrata Pain, Thomas Cunningham, and Suresh Seshadri of Caltech for NASA's Jet Propulsion Laboratory. Further information is contained in a TSP (see page 1).*

*In accordance with Public Law 96-517, the contractor has elected to retain title to this invention. Inquiries concerning rights for its commercial use should be addressed to:*

*Innovative Technology Assets Management  
JPL*

*Mail Stop 202-233  
4800 Oak Grove Drive  
Pasadena, CA 91109-8099  
(818) 354-2240*

*E-mail: iaoffice@jpl.nasa.gov*

*Refer to NPO-40683, volume and number of this NASA Tech Briefs issue, and the page number.*

## Diode-Laser-Based Spectrometer for Sensing Gases

*John H. Glenn Research Center, Cleveland, Ohio*

A diode-laser-based spectrometer has been developed for measuring concentrations of gases and is intended particularly for use in analyzing and monitoring combustion processes under microgravitational

conditions in a drop tower or a spacecraft. This instrument is also well suited for use on Earth in combustion experiments and for such related purposes as fire-safety monitoring and monitoring toxic and flammable gases

in industrial settings.

Of the gas-sensing spectrometers available prior to the development of this instrument, those that were sensitive enough for measuring the combustion gases of interest were too large, re-

quired critical optical alignments, used far too much electrical power, and were insufficiently rugged for use under the severe conditions of spacecraft launch and space flight. In contrast, the present instrument is compact, consumes relatively little power, and is rugged enough to withstand launch vibrations and space flight. In addition, this instrument is characterized by long-term stability, accuracy, and reliability.

The diode laser in this spectrometer is operated in a wavelength-modulation mode. Different gases to be measured can be selected by changing modular laser units. The operation of the laser is controlled by customized, low-power electronic circuitry built around a digital signal-processor board. This customized circuitry also performs acquisition and analysis of data, controls communications, and manages errors.

*This work was done by Joel A. Silver of Southwest Sciences, Inc., for **Glenn Research Center**. Further information is contained in a TSP (see page 1).*

*Inquiries concerning rights for the commercial use of this invention should be addressed to NASA Glenn Research Center, Commercial Technology Office, Attn: Steve Fedor, Mail Stop 4-8, 21000 Brookpark Road, Cleveland, Ohio 44135. Refer to LEW-17546-1.*





## Improved Cathode Structure for a Direct Methanol Fuel Cell

The improvement is intended to reduce the airflow demand.

NASA's Jet Propulsion Laboratory, Pasadena, California

An improved cathode structure on a membrane/electrode assembly has been developed for a direct methanol fuel cell, in a continuing effort to realize practical power systems containing such fuel cells. This cathode structure is intended particularly to afford better cell performance at a low airflow rate.

A membrane/electrode assembly of the type for which the improved cathode structure was developed (see Figure 1) is fabricated in a process that includes brush painting and spray coating of catalyst layers onto a polymer-electrolyte membrane and onto gas-diffusion backings that also act as current collectors. The aforementioned layers are then dried and hot-pressed together. When completed, the membrane/electrode assembly contains (1) an anode containing a fine metal black of Pt/Ru alloy, (2) a membrane made of Nafion 117® or

equivalent (a perfluorosulfonic acid-based hydrophilic, proton-conducting ion-exchange polymer), (3) a cathode structure (in the present case, the improved cathode structure described below), and (4) the electrically conductive gas-diffusion backing layers, which are made of Toray 060™ (or equivalent) carbon paper containing between 5 and 6 weight percent of poly(tetrafluoroethylene).

The need for an improved cathode structure arises for the following reasons: In the design and operation of a fuel-cell power system, the airflow rate is a critical parameter that determines the overall efficiency, cell voltage, and power density. It is desirable to operate at a low airflow rate in order to obtain thermal and water balance and to minimize the size and mass of the system. The performances of membrane/electrode assemblies of prior design are limited at low airflow rates. Methanol crossover increases the required airflow rate. Hence, one way to reduce the required airflow rate is to reduce the effect of methanol crossover. Improvement of the cathode structure — in particular, addition of hy-

drophobic particles to the cathode — has been demonstrated to mitigate the effects of crossover and decrease the airflow required.

The present improved cathode structure and the membrane/electrode assembly of which it is a part differ from prior such structures in the manner in which hydrophobic particles are distributed in the various layers and in the pre-treatment of the membrane. The improved cathode is fabricated in a variant of the fabrication process summarized above. The major steps of this variant of the process as they affect the cathode are the following:

1. The polymer-electrolyte membrane is roughened by use of a 600-grit-abrasive-coated paper.
2. For a membrane area of 25 cm<sup>2</sup>, an ink comprising 0.18 g of Pt catalyst, 0.72 g of Nafion® (5 percent ionomer solution), and 0.40 g of water is applied to the abraded membrane surface by a paintbrush.
3. Air is blown over the painted membrane surface to dry the ink.
4. The gas-diffusion/current-collecting carbon paper is brush-coated with an

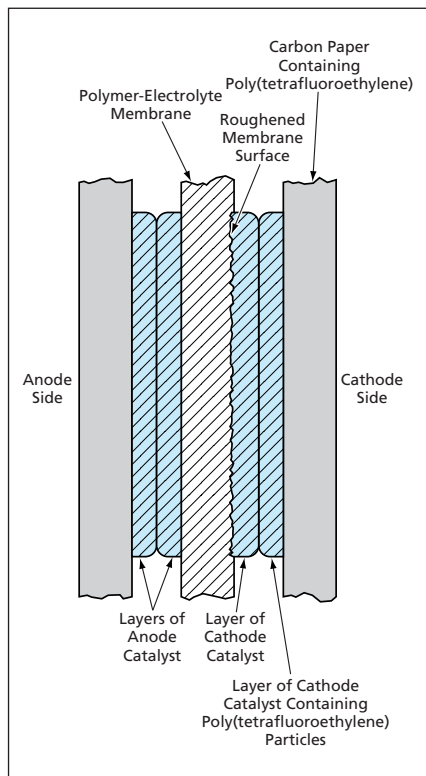


Figure 1. This Membrane/Electrode Assembly resembles prior such assemblies but contains the improved cathode structure described in the text. The layers are not drawn to scale: thicknesses are exaggerated.

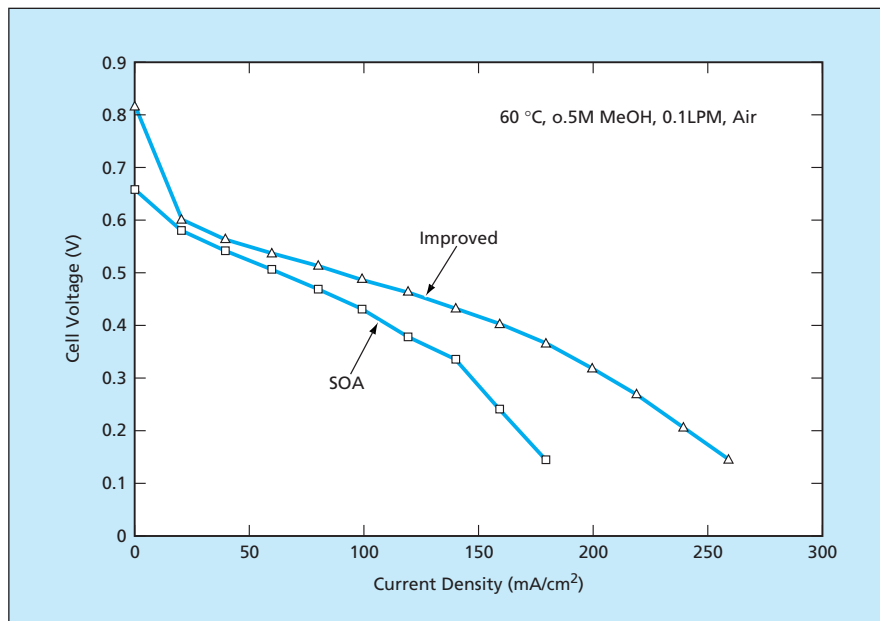


Figure 2. The Performance of the Membrane Electrode Assembly produced with the new process shows improvement from that produced by the state-of-the-art process (SOA) that was used at the time of this development.

ink that contains the ingredients described for step 2, plus 0.035 g of poly(tetrafluoroethylene) particles.

5. The membrane coated with catalyst layer is bonded to the gas-diffusion/current-collecting carbon paper by use of heat and pressure.

The performance of membrane electrode assemblies prepared by the new process is compared with those prepared by the state-of-art (SOA) process in Figure 2. The current density at 0.49 V has been raised from 70 mA/cm<sup>2</sup> to 100 mA/cm<sup>2</sup>. This results in an increase in

power density of 43 percent. At an applied current density of 100 mA/cm<sup>2</sup>, the cell voltage for the SOA cell and improved cell are 0.43 and 0.49, respectively. The increase in cell voltage between the SOA and improved cell resulted in an increase in cell efficiency of 8 percent when the effects of crossover are included.

*This work was done by Thomas Valdez and Sekharipuram Narayanan of Caltech for NASA's Jet Propulsion Laboratory. Further information is contained in a TSP (see page 1).*

*In accordance with Public Law 96-517, the contractor has elected to retain title to this invention. Inquiries concerning rights for its commercial use should be addressed to:*

*Innovative Technology Assets Management  
JPL*

*Mail Stop 202-233  
4800 Oak Grove Drive  
Pasadena, CA 91109-8099  
(818) 354-2240*

*E-mail: iaoffice@jpl.nasa.gov*

*Refer to NPO-30829, volume and number of this NASA Tech Briefs issue, and the page number.*

## X-Band, 17-Watt Solid-State Power Amplifier

**This is a smaller, lighter, less expensive alternative to prior X-band amplifiers.**

*NASA's Jet Propulsion Laboratory, Pasadena, California*

An advanced solid-state power amplifier that can generate an output power of as much as 17 W at a design operating frequency of 8.4 GHz has been designed and constructed as a smaller, lighter, less expensive alternative to traveling-

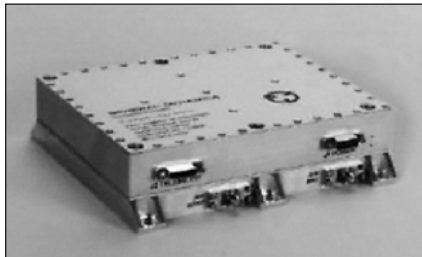


Figure 1. The Complete Amplifier Package has dimensions of 6.75 by 5.25 by 1.75 in. (about 17.1 by 13.3 by 4.4 cm).

wave-tube X-band amplifiers and to prior solid-state X-band power amplifiers of equivalent output power. This amplifier comprises a monolithic microwave integrated circuit (MMIC) amplifier module and a power-converter module integrated into a compact package (see Figure 1).

The amplifier module contains an input variable-gain amplifier (VGA), an intermediate driver stage, a final power stage, and input and output power monitors (see Figure 2). The VGA and the driver amplifier are 0.5- $\mu$ m GaAs-based metal semiconductor field-effect transistors (MESFETs). The final power stage contains four parallel high-efficiency, GaAs-based pseudomorphic high-electron-mobility transistors (PHEMTs). The

gain of the VGA is voltage-variable over a range of 10 to 24 dB. To provide for temperature compensation of the overall amplifier gain, the gain-control voltage is generated by an operational-amplifier circuit that includes a resistor/thermistor temperature-sensing network. The driver amplifier provides a gain of 14 dB to an output power of 27 dBm to drive the four parallel output PHEMTs, each of which is nominally capable of putting out as much as 5 W. The driver output is sent to the input terminals of the four parallel PHEMTs through microstrip power dividers; the outputs of these PHEMTs are combined by microstrip power combiners (which are similar to the microstrip power dividers) to obtain the final output power of 17 W.

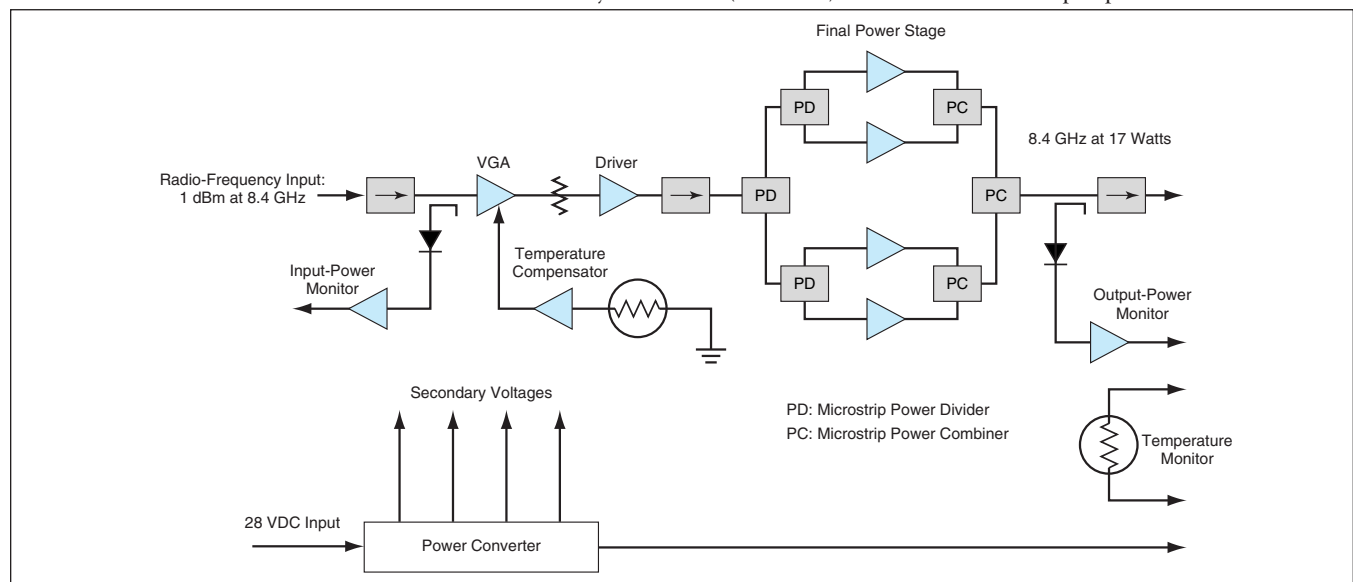


Figure 2. This Block Diagram shows only major functional blocks of the amplifier and power-converter modules.



The power-converter module contains a high-efficiency (nominally 90-percent efficient) DC-to-DC power converter plus analog signal-conditioning circuitry for use in remote monitoring (e.g., telemetry) of temperature, and of radio-frequency input and output power levels. The power converter contains a transformer in a push-pull, pulse-width-modulated buck regulator circuit. Feedback for regulation of power-converter output voltages is provided by a transformer winding that is in addition to the primary and secondary winding. Feedback-loop compen-

sation is provided by an error amplifier and associated resistors and capacitors within the pulse-width modulator. To maximize efficiency, the output voltages are obtained via synchronous rectifiers connected to the secondary winding of the transformer. The ripple in the outputs of the rectifiers is attenuated by use of inductance-capacitance filters.

The output power of 17 W is obtained with a nominal input radio-frequency power of 1 dBm ( $\approx 1.3$  mW) and an input DC power of 59 W. The amplifier and power-converter modules are configured

and stacked in a manner that provides the best thermally conductive path for dissipating heat generated in the final power stage. The amplifier can operate over a temperature range from  $-40$  to  $+70$  °C, from sea-level to Mars' atmosphere and even to a vacuum.

*This work was done by Anthony Mittskus and Ernest Stone of Caltech and William Boger, David Burgess, Richard Honda, and Carl Nuckolls of General Dynamics Decision Systems for NASA's Jet Propulsion Laboratory. Further information is contained in a TSP (see page 1). NPO-30663*

## Improved Anode for a Direct Methanol Fuel Cell

Electrical resistance is decreased and utilization of catalyst is increased.

NASA's Jet Propulsion Laboratory, Pasadena, California

A modified chemical composition has been devised to improve the performance of the anode of a direct methanol fuel cell. The main feature of the modified composition is the incorporation of hydrous ruthenium oxide into the anode structure. This modification can reduce the internal electrical resistance of the cell and increase the degree of utilization of the anode catalyst. As a result, a higher anode current density can be sustained with a smaller amount of anode catalyst. These improvements can translate into a smaller fuel-cell system and higher efficiency of conversion.

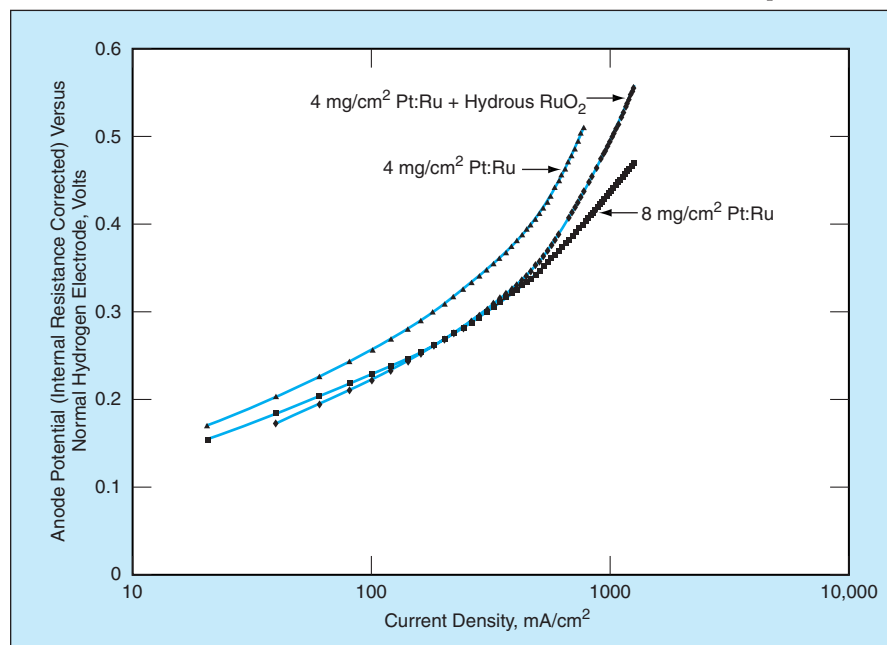
Some background information is helpful for understanding the benefit afforded by the addition of hydrous ruthenium oxide. The anode of a direct methanol fuel cell sustains the electro-oxidation of methanol to carbon dioxide in the reaction  $\text{CH}_3\text{OH} + \text{H}_2\text{O} \rightarrow \text{CO}_2 + 6\text{H}^+ + 6\text{e}^-$ . An electrocatalyst is needed to enable this reaction to occur. The catalyst that offers the highest activity is an alloy of approximately equal numbers of atoms of the noble metals platinum and ruthenium. The anode is made of a composite material that includes high-surface-area Pt/Ru-alloy particles and a proton-conducting ionomeric material. This composite is usu-

ally deposited onto a polymer-electrolyte (proton-conducting) membrane and onto an anode gas-diffusion/current-collector sheet that is subsequently bonded to the proton-conducting membrane by hot pressing.

Heretofore, the areal density of noble-metal catalyst typically needed for high performance has been about  $8 \text{ mg/cm}^2$ . However, not all of the catalyst has been utilized in the catalyzed electro-oxidation reaction. Increasing the degree of utilization of the catalyst would make it possible to improve the performance of the cell for a given catalyst loading and/or reduce the catalyst loading (thereby reducing the cost of the cell).

The use of carbon and possibly other electronic conductors in the catalyst layer has been proposed for increasing the utilization of the catalyst by increasing electrical connectivity between catalyst particles. However, the relatively low density of carbon results in thick catalyst layers that impede the mass transport of methanol to the catalytic sites. Also, the electrical conductivity of carbon is less than  $1/300$ th of typical metals. Furthermore, the polymer-electrolyte membrane material is acidic and most metals are not chemically stable in contact with it. Finally, a material that conducts electrons (but not protons) does not contribute to the needed transport of protons produced in the electro-oxidation reaction.

Hence, what is needed is an additive that is stable in contact with the polymer-electrolyte membrane and that conducts both electrons and protons. Hydrous



These Plots of Anode Overpotential Versus Current Density were obtained in tests of direct methanol fuel cells operated at a temperature of 90 °C and a methanol concentration of 1 M.

ruthenium oxide has these properties. Its density is comparable to that of the platinum-ruthenium catalyst.

A membrane/electrode assembly that had an electrode area of  $25 \text{ cm}^2$  and that included hydrous ruthenium oxide as an anode additive was fabricated to test this concept. An ink having a consistency suitable for painting was prepared by sonicating a mixture of 0.14 g of ruthenium oxide, 0.72 g of Nafion® ionomer solution, and 0.40 g of water. A layer of the ink was applied to a polymer-electrolyte membrane. A layer containing the Pt/Ru catalyst at a density of  $4 \text{ mg/cm}^2$  was applied to the gas-diffusion/current-collector sheet. The membrane and the sheet were bonded in a hot press.

A fuel cell containing this membrane/electrode assembly containing the hydrous ruthenium oxide additive

was fabricated and tested. Also fabricated and tested were two fuel cells not containing the additive — one having a catalyst loading of  $4 \text{ mg/cm}^2$ , the other having a catalyst loading of  $8 \text{ mg/cm}^2$ . Some results of the tests are plotted in the figure. These results show that at current densities up to a few hundred  $\text{mA/cm}^2$ , the polarization of the anode containing the additive was low — comparable to that of the anode that contained twice as much catalyst without the additive. In effect, these results can be interpreted as signifying that the degree of utilization of the anode catalyst was approximately doubled. The overall internal resistance of the cell containing the additive was 4.6 mW, which is among the lowest values yet observed for cells of the same size; this attests to the high

protonic and electronic conductivity of hydrous ruthenium oxide.

*This work was done by Thomas Valdez and Sekharipuram Narayanan of Caltech for NASA's Jet Propulsion Laboratory. Further information is contained in a TSP (see page 1).*

*In accordance with Public Law 96-517, the contractor has elected to retain title to this invention. Inquiries concerning rights for its commercial use should be addressed to:*

*Innovative Technology Assets Management  
JPL*

*Mail Stop 202-233*

*4800 Oak Grove Drive*

*Pasadena, CA 91109-8099*

*(818) 354-2240*

*E-mail: iaoffice@jpl.nasa.gov*

*Refer to NPO-30830, volume and number of this NASA Tech Briefs issue, and the page number.*



## Tools for Designing and Analyzing Structures

Structural Design and Analysis Toolset is a collection of approximately 26 Microsoft Excel spreadsheet programs, each of which performs calculations within a different subdiscipline of structural design and analysis. These programs present input and output data in user-friendly, menu-driven formats. Although these programs cannot solve complex cases like those treated by larger finite element codes, these programs do yield quick solutions to numerous common problems more rapidly than the finite element codes, thereby making it possible to quickly perform multiple preliminary analyses — e.g., to establish approximate limits prior to detailed analyses by the larger finite element codes. These programs perform different types of calculations, as follows:

1. determination of geometric properties for a variety of standard structural components;
2. analysis of static, vibrational, and thermal-gradient loads and deflections in certain structures (mostly beams and, in the case of thermal-gradients, mirrors);
3. kinetic energies of fans;
4. detailed analysis of stress and buckling in beams, plates, columns, and a variety of shell structures; and
5. temperature dependent properties of materials, including figures of merit that characterize strength, stiffness, and deformation response to thermal gradients.

*This program was written by Paul L. Luz of Marshall Space Flight Center. For further information, contact Sammy Nabors, MSFC Commercialization Assistance Lead, at sammy.a.nabors@nasa.gov. Refer to MFS-31797.*

## Interactive Display of Scenes With Annotations

ThreeDView is a computer program that enables high-performance interactive display of real-world scenes with annotations. ThreeDView was developed primarily as a component of the Science Activity Planner (SAP) software, wherein it is to be used to display annotated images of terrain acquired by exploratory robots on Mars and possibly other remote

planets. The images can be generated from sets of multiple-texture image data in the Visible Scalable Terrain (ViSTa) format, which was described in “Format for Interchange and Display of 3D Terrain Data” (NPO-30600) *NASA Tech Briefs*, Vol. 28, No. 12 (December 2004), page 25. In ThreeDView, terrain data can be loaded rapidly, the geometric level of detail and texture resolution can be selected, false colors can be used to represent scientific data mapped onto terrain, and the user can select among navigation modes. ThreeDView consists largely of modular Java software components that can easily be reused and extended to produce new high-performance, application-specific software systems for displaying images of three-dimensional real-world scenes.

*This program was written by Marsette Vona, Mark Powell, Paul Backes, Jeffrey Norris, and Robert Steinke of Caltech for NASA’s Jet Propulsion Laboratory. Further information is contained in a TSP (see page 1).*

*This software is available for commercial licensing. Please contact Don Hart of the California Institute of Technology at (818) 393-3425. Refer to NPO-30675.*

## Solving Common Mathematical Problems

Mathematical Solutions Toolset is a collection of five software programs that rapidly solve some common mathematical problems. The programs consist of a set of Microsoft Excel worksheets. The programs provide for entry of input data and display of output data in a user-friendly, menu-driven format, and for automatic execution once the input data has been entered. The programs perform the following calculations:

1. “Definite Integral Evaluator 1.0” calculates the definite integral of a user-specified function  $y = f(x)$  between user-specified limits for the lower and upper bands. The program will also plot the function.
2. Solve for  $X$  in the matrix equation  $AX = B$ , where  $A$  is a  $2 \times 2$ ,  $3 \times 3$ , or  $6 \times 6$  matrix of constant coefficients,  $X$  is the matrix of unknown independent values, and  $B$  is the matrix of dependant values.
3. “Cubic Equation Solver” calculates the real and imaginary roots,  $x$ , of the cubic equation  $x^3 + ax^2 + bx + c = 0$ .

4. Given a pair of vectors specified in terms of their Cartesian components, the Vector Calculator program calculates their scalar product, their vector product, the unit vectors, and the angle between the vectors.
5. “Unit Conversions” will convert between the English and metric values of the most commonly used units for length, volume, velocity, mass, density, force, pressure, energy, power, temperature, and thermal energy.

*This program was written by Paul L. Luz of Marshall Space Flight Center. For further information, contact Sammy Nabors, MSFC Commercialization Assistance Lead, at sammy.a.nabors@nasa.gov. Refer to MFS-31794.*

## Tools for Basic Statistical Analysis

Statistical Analysis Toolset is a collection of eight Microsoft Excel spreadsheet programs, each of which performs calculations pertaining to an aspect of statistical analysis. These programs present input and output data in user-friendly, menu-driven formats, with automatic execution. The following types of calculations are performed:

- Descriptive statistics are computed for a set of data  $x(i)$  ( $i = 1, 2, 3 \dots$ ) entered by the user.
- “Normal Distribution Estimates” will calculate the statistical value that corresponds to cumulative probability values, given a sample mean and standard deviation of the normal distribution.
- “Normal Distribution from two Data Points” will extend and generate a cumulative normal distribution for the user, given two data points and their associated probability values.
- Two programs perform two-way analysis of variance (ANOVA) with no replication or generalized ANOVA for two factors with four levels and three repetitions.
- “Linear Regression-ANOVA” will curve-fit data to the linear equation  $y=f(x)$  and will do an ANOVA to check its significance.
- Two multiple regression programs will do statistical analysis on test data that includes more than one predictor and will perform curve-fitting of the data to either the equation  $y = f(x_1, x_2)$  or  $y = f(x_1, x_2, x_3, x_4)$ .

*This program was written by Paul L. Luz of Marshall Space Flight Center. For further information, contact Sammy Nabors, MSFC Commercialization Assistance Lead, at sammy.a.nabors@nasa.gov. Refer to MFS-31796.*

### Program Calculates Forces in Bolted Structural Joints

A FORTRAN 77 computer program calculates forces in bolts in the joints of structures. This program is used in conjunction with the NASTRAN finite-element structural-analysis program. A mathematical model of a structure is first created by approximating its load-bearing members with representative finite elements, then NASTRAN calculates the forces and moments that each finite element contributes to grid points located throughout the structure. The user selects the finite elements that correspond to structural members that contribute loads to the joints of interest, and identifies the grid point nearest to each such joint. This program reads the pertinent NASTRAN output, combines the forces and moments from the contributing elements to determine the resultant force and moment acting at each proximate grid point, then transforms the forces and moments from these grid points to the centroids of the affected joints. Then the program uses these joint loads to obtain the axial and

shear forces in the individual bolts. The program identifies which bolts bear the greatest axial and/or shear loads. The program also performs a “fail-safe” analysis in which the foregoing calculations are repeated for a sequence of cases in which each fastener, in turn, is assumed not to transmit an axial force.

*This program was written by Daniel A. Buder of The Boeing Company for Johnson Space Center.*

*Title to this invention, covered by U.S. Patent No. 5,884,232 has been waived under the provisions of the National Aeronautics and Space Act (42 U.S.C. 2457 (f)). Inquiries concerning licenses for its commercial development should be addressed to:*

*The Boeing Company  
Rocketdyne Propulsion & Power  
6633 Canoga Avenue  
P.O. Box 7922*

*Canoga Park, CA 91309-7922*

*Phone: (818) 586-1367*

*Fax: (818) 586-2833*

*E-mail: danielle.bartoli@boeing.com*

*Refer to MSC-23121, volume and number of this NASA Tech Briefs issue, and the page number.*

### Integrated Structural Analysis and Test Program

An integrated structural-analysis and structure-testing computer program is being developed in order to:

- Automate repetitive processes in testing and analysis;
- Accelerate pre-test analysis;
- Accelerate reporting of tests;
- Facilitate planning of tests;
- Improve execution of tests;
- Create a vibration, acoustics, and shock test database; and
- Integrate analysis and test data.

The software package includes modules pertaining to sinusoidal and random vibration, shock and time replication, acoustics, base-driven modal survey, and mass properties and static/dynamic balance. The program is commanded by use of ActiveX controls. There is minimal need to generate command lines. Analysis or test files are selected by opening a Windows Explorer display. After selecting the desired input file, the program goes to a so-called analysis data process or test data process, depending on the type of input data. The status of the process is given by a Windows status bar, and when processing is complete, the data are reported in graphical, tubular, and matrix form.

*This work was done by Daniel Kaufman of Goddard Space Flight Center. Further information is contained in a TSP (see page 1).*

*This invention is owned by NASA, and a patent application has been filed. Inquiries concerning nonexclusive or exclusive license for its commercial development should be addressed to the Patent Counsel, Goddard Space Flight Center; (301) 286-7351. Refer to GSC-14775-1.*



## Molybdate Coatings for Protecting Aluminum Against Corrosion

These coatings show promise, but further development is needed.

John F. Kennedy Space Center, Florida

Conversion coatings that comprise mixtures of molybdates and several additives have been subjected to a variety of tests to evaluate their effectiveness in protecting aluminum and alloys of aluminum against corrosion. Molybdate conversion coatings are under consideration as replacements for chromate conversion coatings, which have been used for more than 70 years. The chromate coatings are highly effective in protecting aluminum and its alloys against corrosion but are also toxic and carcinogenic. Hexavalent molybdenum and, hence, molybdates containing hexavalent molybdenum, have received attention recently as replacements for chromates because molybdates mimic chromates in a variety of applications but exhibit significantly lower toxicity.

The tests were performed on six proprietary formulations of molybdate conversion coatings, denoted formulations A through F, on panels of aluminum alloy 2024-T3. A bare alloy panel was also included in the tests. The tests included

electrochemical impedance spectroscopy (EIS), measurements of corrosion potentials, scanning electron microscopy (SEM) with energy-dispersive spectroscopy (EDS), and x-ray photoelectron spectroscopy (XPS).

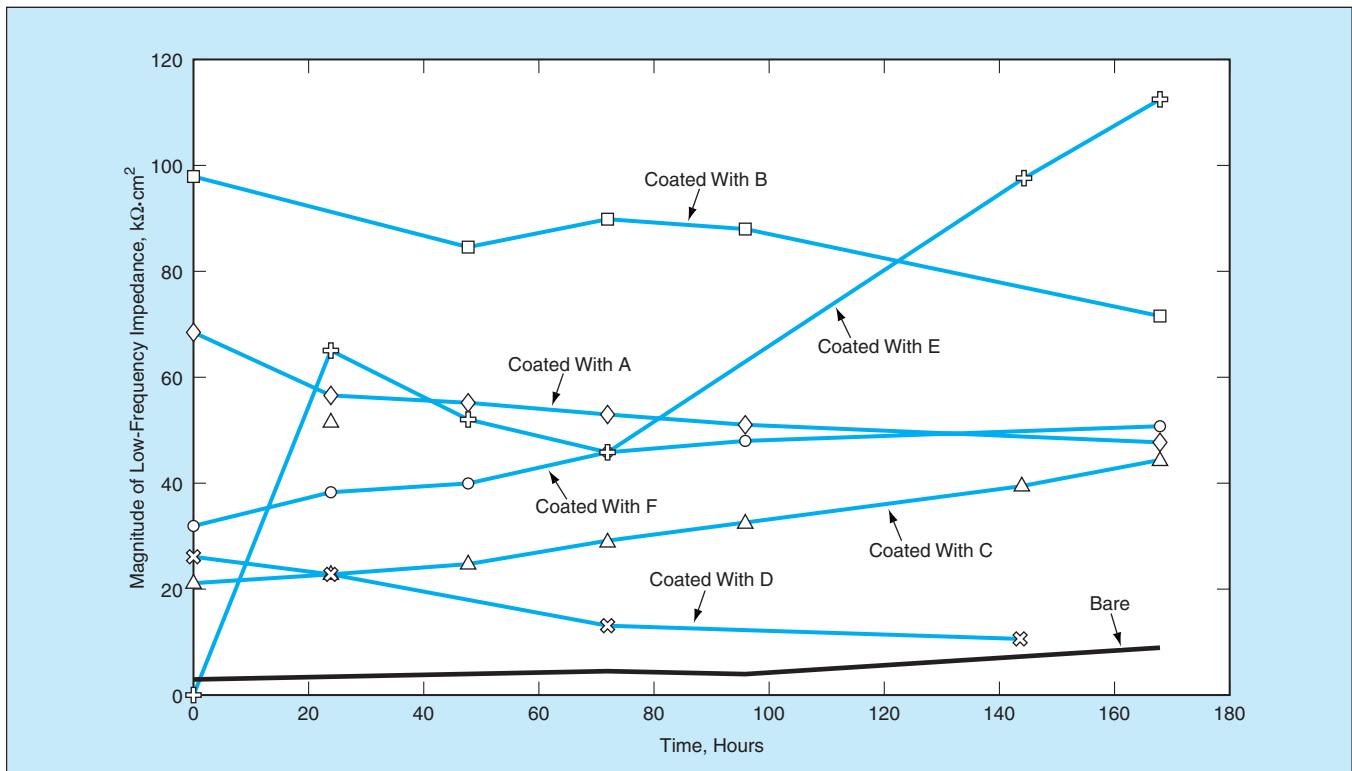
The corrosion-potential and EIS measurement data were gathered at several intervals during immersion in an aqueous NaCl solution for a total time of two weeks. Nyquist and Bode plots of the data were obtained. The corrosion potentials of the conversion-coated panels were found to increase during the first 24 hours and thereafter subside slightly, approaching steady values. The corrosion-potential measurements indicated that three of the proprietary formulations exerted a protective effect on the alloy. The EIS data on all the conversion-coated alloy specimens were characterized by impedance magnitudes greater than those of the bare alloy specimen at all frequencies and times for which measurements were performed (see figure). This characteristic indicates that the

molybdate conversion coatings contribute some resistance to corrosion.

SEM images showed cracks in the coatings and cubic crystals believed to be calcium carbonate. EDS revealed high concentrations of aluminum, oxygen, and calcium but did not reveal any molybdenum on the panels. XPS indicated the presence of less than 0.01 atomic percent molybdenum on the surfaces of the coatings.

Overall, the test data have been interpreted as signifying that molybdate conversion coatings show promise for protecting aluminum and its alloys against corrosion, but that further development will be necessary to attain protection equal to that afforded by chromate conversion coatings.

This work was done by Luz Marina Calle and Louis G. MacDowell of Kennedy Space Center. For further information, contact the Kennedy Commercial Technology Office at 321-867-8130. KSC-12346



The Magnitude of Impedance at a frequency of 0.05 Hz was measured on each of the seven specimens as a function of immersion time.

# Synthesizing Diamond From Liquid Feedstock

Precise proportioning of feedstock gases is not necessary.

Goddard Space Flight Center, Greenbelt, Maryland

A relatively economical method of chemical vapor deposition (CVD) has been developed for synthesizing diamond crystals and films. Unlike prior CVD methods for synthesizing diamond, this method does not require precisely proportioned flows of compressed gas feedstocks or the use of electrical discharges to decompose the feedstocks to obtain free radicals needed for deposition chemical reactions. Instead, the feedstocks used in this method are mixtures of common organic liquids that can be prepared in advance, and decomposition of feedstock vapors is effected simply by heating.

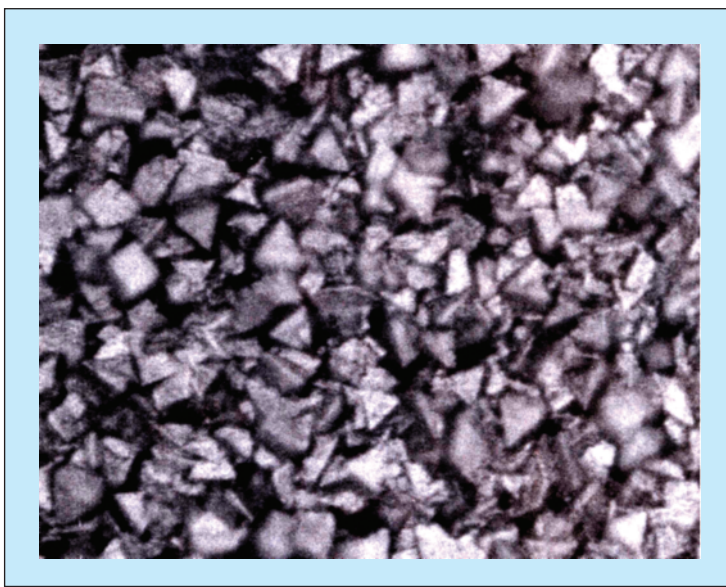
The feedstock used in this method is a solution comprising between 90 and 99 weight percent of methanol and the balance of one or more other oxyhydrocarbons that could include ethanol, isopropanol, and/or acetone. This mixture of compounds is chosen so that dissociation of molecules results in the desired proportions of carbon-containing radicals (principally,  $\text{CH}_3$ ) and of OH, H, and O radicals. Undesirably, the CVD temperature and pressure conditions thermodynamically favor the growth of graphite over the growth of diamond. The H radicals are desirable because they help to stabilize the growing surface of diamond by shifting the thermodynamic balance toward favoring the growth of diamond. The OH and O radicals are desirable because they preferentially etch graphite and other non-diamond carbon, thereby helping to ensure the net deposition of pure diamond. The non-methanol compounds are included in the solution because (1) methanol contains equal numbers of C and O atoms; (2) an excess of C over O is needed to obtain net deposition of diamond; and (3) the non-methanol molecules contain multiple carbon atoms for each oxygen atom and thus supply the needed excess carbon.

A typical apparatus used in this method includes a reservoir containing the feedstock liquid and a partially evacuated stainless-steel reaction chamber. The reservoir is connected to the chamber via tubing and a needle valve

becomes heated by the filament to a deposition temperature in the approximate range of 800 to 1,000 °C.

The composition of the feedstock must be chosen in conjunction with other operational parameters to obtain a high-quality diamond deposit. When the feedstock comprises methanol alone, no diamond is deposited on the substrate and there is too much oxidation of the hot filament and consequent gradual reduction in the diameter of the filament. When the liquid contains too much ethanol, isopropanol, or acetone, the filament becomes coated with graphite and thus swollen. When the substrate is placed too close to the filament, the concentration of the etchant radicals is too high, preventing net deposition. In experiments, it was found that choice of an optimum combination of composition of the feedstock, filament temperature, filament-to-substrate distance, and vapor pressure results in the deposition of high-quality diamond (see figure) on the substrate. Moreover, it was found that if the optimum vapor pressure is established in the chamber before heating the filament, then the filament becomes coated with a thin layer of carbon that prevents erosion of the filament by the etchant radicals during the deposition process.

When the liquid contains too much ethanol, isopropanol, or acetone, the filament becomes coated with graphite and thus swollen. When the substrate is placed too close to the filament, the concentration of the etchant radicals is too high, preventing net deposition. In experiments, it was found that choice of an optimum combination of composition of the feedstock, filament temperature, filament-to-substrate distance, and vapor pressure results in the deposition of high-quality diamond (see figure) on the substrate. Moreover, it was found that if the optimum vapor pressure is established in the chamber before heating the filament, then the filament becomes coated with a thin layer of carbon that prevents erosion of the filament by the etchant radicals during the deposition process.



This **Optical Micrograph** at a magnification of about 500 shows diamond grains in a layer  $\approx 10 \mu\text{m}$  thick on a silicon substrate. The diamond was deposited using a feedstock solution of about 4 weight percent ethanol in methanol, a vapor pressure of 40 torr ( $\approx 5 \text{ kPa}$ ), a 1.5-mm-diameter tungsten filament wound in a spiral of  $\approx 2.5 \text{ cm}$  diameter and heated by a current of 110 A, and other deposition conditions as described above.

or other suitable flow controller. When the liquid enters the low-pressure environment inside the chamber, it evaporates to form a vapor mixture of the same chemical composition. In addition to the inlet for the feedstock liquid, the chamber is fitted with an outlet connected to a vacuum pump (not shown) through a throttle valve (also not shown) that is automatically controlled to keep the pressure at or near the required value throughout the deposition process.

Inside the chamber, a spiral filament made of tungsten, tantalum, graphite, or other high-melting-temperature material is electrically heated to a temperature  $>2,000 \text{ }^\circ\text{C}$  — high enough to cause dissociation of vapor molecules into the aforementioned radicals. A deposition substrate — typically, a diamond-polished silicon wafer about 2.5 cm square — is positioned about 2 cm away from the filament. The exact location of the substrate is chosen so that the substrate

temperature, filament-to-substrate distance, and vapor pressure results in the deposition of high-quality diamond (see figure) on the substrate. Moreover, it was found that if the optimum vapor pressure is established in the chamber before heating the filament, then the filament becomes coated with a thin layer of carbon that prevents erosion of the filament by the etchant radicals during the deposition process.

*This work was done by Yonhua Tzeng of Auburn University for Goddard Space Flight Center.*

*In accordance with Public Law 96-517, the contractor has elected to retain title to this invention. Inquiries concerning rights for its commercial use should be addressed to:*

*Auburn University  
Office of Technology Transfer  
309 Samford Hall*

*Auburn University, AL 36849*

*Refer to GSC-14754-1, volume and number of this NASA Tech Briefs issue, and the page number.*



# Modifying Silicates for Better Dispersion in Nanocomposites

Processability and final material properties are improved.

*John H. Glenn Research Center, Cleveland, Ohio*

An improved chemical modification has been developed to enhance the dispersion of layered silicate particles in the formulation of a polymer/silicate nanocomposite material. The modification involves, among other things, the co-exchange of an alkyl ammonium ion and a monoprotated diamine with interlayer cations of the silicate. The net overall effects of the improved chemical modification are to improve processability of the nanocomposite and maximize the benefits of dispersing the silicate particles into the polymer.

Some background discussion is necessary to give meaning to a description of this development. Polymer/silicate nanocomposites are also denoted polymer/clay composites because the silicate particles in them are typically derived from clay particles. Particles of clay comprise layers of silicate platelets separated by gaps called "galleries." The platelet thickness is 1 nm. The length varies from 30 nm to 1  $\mu\text{m}$ , depending on the silicate. In order to fully realize the benefits of polymer/silicate nanocomposites, it is necessary to ensure that the

platelets become dispersed in the polymer matrices. Proper dispersion can impart physical and chemical properties that make nanocomposites attractive for a variety of applications.

In order to achieve nanometer-level dispersion of a layered silicate into a polymer matrix, it is typically necessary to modify the interlayer silicate surfaces by attaching organic functional groups. This modification can be achieved easily by ion exchange between the interlayer metal cations found naturally in the silicate and protonated organic cations — typically protonated amines. Long-chain alkyl ammonium ions are commonly chosen as the ion-exchange materials because they effectively lower the surface energies of the silicates and ease the incorporation of organic monomers or polymers into the silicate galleries. This completes the background discussion.

In the present improved modification of the interlayer silicate surfaces, the cation exchange strengthens the polymer/silicate interface and ensures irreversible separation of the silicate layers. One way in which it does this is to essen-

tially tether one amine of each diamine molecule to a silicate surface, leaving the second amine free for reaction with monomers during the synthesis of a polymer. In addition, the incorporation of alkyl ammonium ions into the galleries at low concentration helps to keep low the melt viscosity of the oligomer formed during synthesis of the polymer and associated processing — a consideration that is particularly important in the case of a highly cross-linked, thermosetting polymer. Because of the chemical bonding between the surface-modifying amines and the monomers, even when the alkyl ammonium ions become degraded at high processing temperature, the silicate layers do not aggregate and, hence, nanometer-level dispersion is maintained.

*This work was done by Sandi Campbell of Glenn Research Center. Further information is contained in a TSP (see page 1).*

*Inquiries concerning rights for the commercial use of this invention should be addressed to NASA Glenn Research Center, Commercial Technology Office, Attn: Steve Fedor, Mail Stop 4-8, 21000 Brookpark Road, Cleveland, Ohio 44135. Refer to LEW-17339.*





## ✦ Powder-Collection System for Ultrasonic/Sonic Drill/Corer

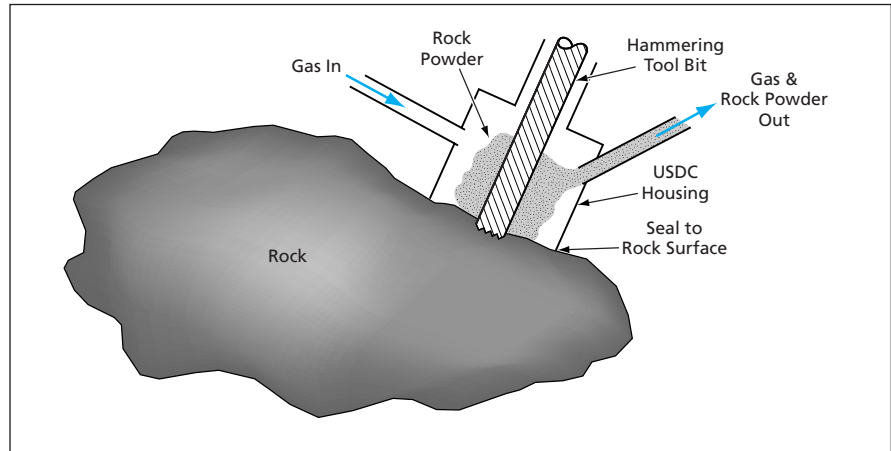
**Powder is blown from the drill/rock interface to sampling locations.**

*NASA's Jet Propulsion Laboratory, Pasadena, California*

A system for collecting samples of powdered rock has been devised for use in conjunction with an ultrasonic/sonic drill/corer (USDC)— a lightweight, low-power apparatus designed to cut into, and acquire samples of, rock or other hard material for scientific analysis. The USDC was described in "Ultrasonic/Sonic Drill/Corers With Integrated Sensors" (NPO-20856), *NASA Tech Briefs*, Vol. 25, No. 1 (January 2001), page 38. To recapitulate: The USDC includes a drill bit, corer, or other tool bit, in which ultrasonic and sonic vibrations are excited by an electronically driven piezoelectric actuator. The USDC advances into the rock or other material of interest by means of a hammering action and a resulting chiseling action at the tip of the tool bit. The hammering and chiseling actions are so effective that unlike in conventional twist drilling, a negligible amount of axial force is needed to make the USDC advance into the material. Also unlike a conventional twist drill, the USDC operates without need for torsional restraint, lubricant, or a sharp bit.

The USDC generates powder as a byproduct of the drilling or coring process. The purpose served by the present sample-collection system is to remove the powder from the tool-bit/rock interface and deliver the powder to one or more designated location(s) for analysis or storage.

The sample-collection system includes parts that are integrated into the USDC



**Powdered Rock** is generated by the hammering action of the tool bit, then entrained in a high-pressure pulse of gas flowing from the inlet, through the outlet, to one or more location(s) for analysis or storage.

(see figure). The USDC is designed so that when the tool bit is brought into contact with the rock, a circular bellows or knife-edge seal at the lower end of the USDC housing is also pressed against the rock, partially sealing the volume enclosed by the USDC housing and the rock face. From time to time during operation of the tool bit, a high-pressure pulse of gas is blown into the volume through an inlet. The resulting flow of gas entrains particles of powder and carries them away through an outlet.

A screen along the path of the powder/gas mixture is used to trap particles above a predetermined size while allowing

acceptably small particles to proceed. The powder can then be further processed in any of several ways. For example, it can be trapped on a porous or adhesive tape for delivery to an instrument or for storage, mixed with fluids by use of a sonicator, or blown into a heating chamber for thermal treatment and analysis.

*This work was done by Stewart Sherrit, Yoseph Bar-Cohen, Xiaoqi Bao, and Zensheu Chang of Caltech for NASA's Jet Propulsion Laboratory and by David Blake of Ames Research Center and Charles Bryson of Bryson Consulting for Ames Research Center. Further information is contained in a TSP (see page 1). NPO-40564*

## ✦ Semiautomated, Reproducible Batch Processing of Soy

**Processing conditions are selectable and are consistent from batch to batch.**

*Lyndon B. Johnson Space Center, Houston, Texas*

A computer-controlled apparatus processes batches of soybeans into one or more of a variety of food products, under conditions that can be chosen by the user and reproduced from batch to batch. Examples of products include soy milk, tofu, okara (an insoluble protein and fiber byproduct of soy milk), and whey. Most processing steps take place without intervention by

the user. This apparatus was developed for use in research on processing of soy. It is also a prototype of other soy-processing apparatuses for research, industrial, and home use.

Prior soy-processing equipment includes household devices that automatically produce soy milk but do not automatically produce tofu. The designs of

prior soy-processing equipment require users to manually transfer intermediate solid soy products and to press them manually and, hence, under conditions that are not consistent from batch to batch. Prior designs do not afford choices of processing conditions: Users cannot use previously developed soy-processing equipment to investigate the

effects of variations of techniques used to produce soy milk (e.g., cold grinding, hot grinding, and pre-cook blanching) and of such process parameters as cooking times and temperatures, grinding times, soaking times and temperatures, rinsing conditions, and sizes of particles generated by grinding. In contrast, the present apparatus is amenable to such investigations.

The apparatus (see figure) includes a processing tank and a jacketed holding or coagulation tank. The processing tank can be capped by either of two different heads and can contain either of two different insertable mesh baskets. The first head includes a grinding blade and heating elements. The second head includes an automated press piston. One mesh basket, designated the okara basket, has oblong holes with a size equivalent to about 40 mesh [40 openings per inch ( $\approx 16$  openings per cen-

timeter)]. The second mesh basket, designated the tofu basket, has holes of 70 mesh [70 openings per inch ( $\approx 28$  openings per centimeter)] and is used in conjunction with the press-piston head. Supporting equipment includes a soy-milk heat exchanger for maintaining selected coagulation temperatures, a filter system for separating okara from other particulate matter and from soy milk, two pumps, and various thermocouples, flowmeters, level indicators, pressure sensors, valves, tubes, and sample ports.

A typical process carried out in this apparatus comprises the following steps:

1. Dry soybeans are placed into the okara basket of the processing tank.
2. The grinding/heating head is put in place, and a drain valve in the tank closes automatically.
3. Water is added to the tank automatically, and the beans are soaked for a programmed time.

4. The drain valve opens automatically to dump the soaking water.

5. The beans are rinsed and drained automatically a selected number of times, each time using a selected amount at a selected temperature.

6. The valve closes, and a selected amount of water at a selected temperature is added automatically. The beans can then be cooked, blanched, and/or ground as chosen by the user. For the sake of example only, the subsequent steps are based on a process known in the soy industry as the Illinois cook process.

7. The beans are blanched for a selected time.

8. Blanching stops automatically and the valve opens, draining the blanching water.

9. The beans are automatically rinsed with cold water, which is then drained.

10. The valve closes. A selected amount of water chilled to a selected temperature is added to the beans automatically.

11. The beans are automatically ground and cooked as user has specified.

12. The user removes the grinder/heater head and replaces it with the press head.

13. Warm water automatically begins to circulate in the holding or coagulation tank.

14. Chilled water is fed to the heat exchanger.

15. The valve opens, and soy milk is automatically pumped through the heat exchanger and selected filters. The soy milk reaches the holding tank at a specified temperature, coagulant is added, and the solution remains at that temperature until coagulation is complete.

16. During coagulation, the press head and okara basket are removed from the processing tank, then the press head is reinserted with the tofu basket.

17. Once coagulation is complete, the mixture is made to flow back into the processing tank.

18. The piston is actuated to press the tofu according to the user's specification.

19. The piston is retracted, then the user removes the head, retrieves the basket, and adjusts the bottom of the basket to release the tofu.

*This work was done by Mary Toerne, Ivan W. Byford, Jack W. Chastain, and Beverly E. Swango of Johnson Engineering Corp. for Johnson Space Center. For further information, contact the Johnson Commercial Technology Office at (281) 483-3809. MSC-23313*



This **Laboratory Apparatus** is a prototype of scientific, industrial, and household soy-processing systems for processing batches of soy under selectable, reproducible conditions.





## Hydrogen Peroxide Enhances Removal of $\text{NO}_x$ From Flue Gases

Radicals from homogeneous decomposition of  $\text{H}_2\text{O}_2$  react with unscrubbable NO to produce scrubbable gases.

John F. Kennedy Space Center, Florida

Pilot scale experiments have demonstrated a method of reducing the amounts of oxides of nitrogen ( $\text{NO}_x$ ) emitted by industrial boilers and power-plant combustors that involves (1) injection of  $\text{H}_2\text{O}_2$  into flue gases and (2) treatment of the flue gases by caustic wet scrubbing like that commonly used to remove  $\text{SO}_2$  from combustion flue gases. Heretofore, the method most commonly used for removing  $\text{NO}_x$  from flue gases has been selective catalytic reduction (SCR), in which the costs of both installation and operation are very high. After further development, the present method may prove to be an economically attractive alternative to SCR.

The primary constituent of  $\text{NO}_x$  is NO. Although the nitrogen acid gases  $\text{HNO}_2$  and  $\text{HNO}_3$  (and, to a lesser extent,  $\text{NO}_2$ ) can be removed from flue gas by caustic scrubbing, NO is almost completely insoluble and thus not scrubbable. If, however, the NO in  $\text{NO}_x$  could be economically converted to  $\text{HNO}_2$  and  $\text{HNO}_3$ , then scrubbing could be an effective means for removing  $\text{NO}_x$ .

NO can be oxidized to  $\text{HNO}_2$ ,  $\text{HNO}_3$ , and  $\text{NO}_2$  at low to moderate flue-gas temperatures by use of hydroxyl radicals (OH). In the present method, the OH needed for oxidation of NO is generated by thermal decomposition of the  $\text{H}_2\text{O}_2$  injected into the flue gas.

For efficiency, it is necessary to maximize the proportion of OH and  $\text{HO}_2$  radicals, relative to other products of decomposition of  $\text{H}_2\text{O}_2$ . In particular, it is necessary to suppress a competing reaction in which  $\text{H}_2\text{O}_2$  decomposes into water and oxygen. This competing reaction occurs readily at surfaces. In general, peroxides are preserved at acidic surfaces and are decomposed at basic ones. Experiments have shown that the incidence of the competing decomposition into  $\text{H}_2\text{O}$  and O can be reduced by treating reactor surfaces with boric acid to render them acidic.

In one of several sets of experiments to demonstrate the feasibility of the method, the optimum temperature for conversion of NO to  $\text{HNO}_2$ ,  $\text{HNO}_3$ , and

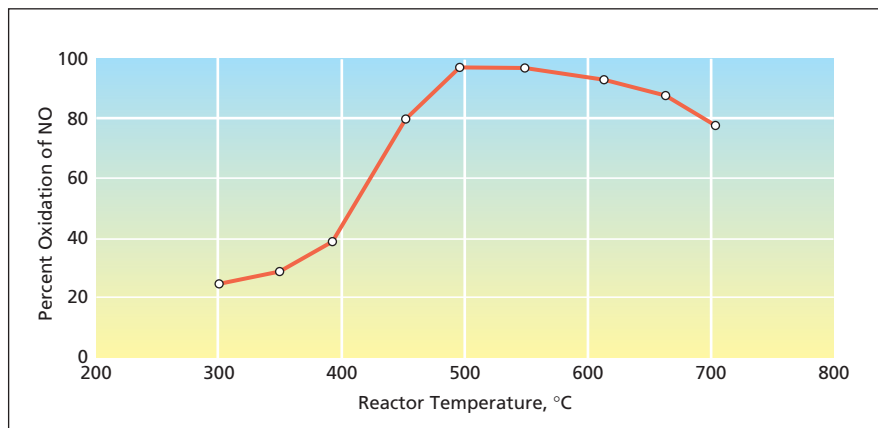


Figure 1. The Conversion of NO by oxidation to other species was measured as a function of reactor temperature. The reactor inlet conditions for the points shown here were 400 ppm NO and 400 ppm  $\text{H}_2\text{O}_2$  for an  $\text{H}_2\text{O}_2$ :NO molar ratio of 1.0:1.0.

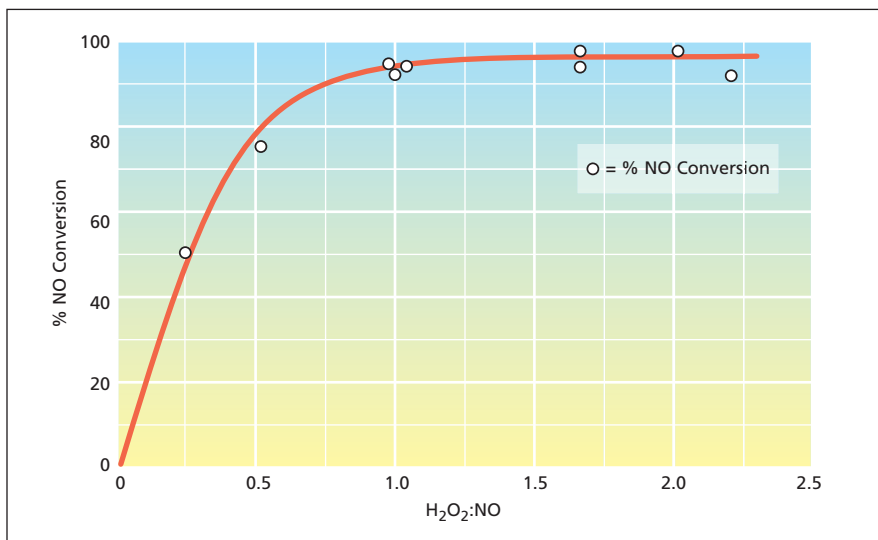


Figure 2. The Outlet Concentration of NO was significantly reduced when  $\text{H}_2\text{O}_2$  was injected. At 500 °C, 400 ppm NO, and various inlet concentrations of  $\text{H}_2\text{O}_2$  (represented as  $\text{H}_2\text{O}_2$ : $\text{NO}_x$  molar ratios), 90-percent conversion of NO was achieved at the reactor outlet for a molar ratio of 1:1.

$\text{NO}_2$  by use of injected  $\text{H}_2\text{O}_2$  was found to be about 500 °C (see Figure 1).

A study performed under the guidelines of the EPA, EPRI comparing the economics of SCR and the experimental  $\text{H}_2\text{O}_2$ -injection/scrubbing method was conducted for a design base case and a variety of alternative cases. This study illustrated the tradeoff between capital and operating costs for the two methods. The single largest factor in determining

the total cost of one method relative to the other method was found to be the  $\text{H}_2\text{O}_2$ : $\text{NO}_x$  molar ratio. At the  $\text{H}_2\text{O}_2$ : $\text{NO}_x$  molar ratio of 1.92, which was previously demonstrated in the laboratory, the  $\text{H}_2\text{O}_2$ -injection/scrubbing method was shown to be uneconomical. However, it was also concluded that the molar ratio in a full-size coal-fired power plant could be lower than that found in the laboratory, and that on the basis of all the assump-

tions of the study, at an H<sub>2</sub>O<sub>2</sub>:NO<sub>x</sub> molar ratio of 1.37, the H<sub>2</sub>O<sub>2</sub>-injection/scrubbing method could be an economically feasible alternative to SCR.

Pilot-scale tests run at Kennedy Space Center demonstrated the feasibility and competitiveness of this new technology. The H<sub>2</sub>O<sub>2</sub> to NO molar ratio, at 500 °C

shown to achieve a NO conversion efficiency of > 90 percent was 1:1, which is significantly lower than the required 1.37:1 (See Figure 2).

*This work was done by Michelle M. Collins of Kennedy Space Center and C. David Cooper and Christian A. Clausen III of the University of Central Florida.*

*This invention is owned by NASA, and a patent application has been filed. Inquiries concerning nonexclusive or exclusive license for its commercial development should be addressed to the Technology Commercialization Office, Kennedy Space Center, (321) 867-1463. Refer to KSC-12056.*

## Subsurface Ice Probe

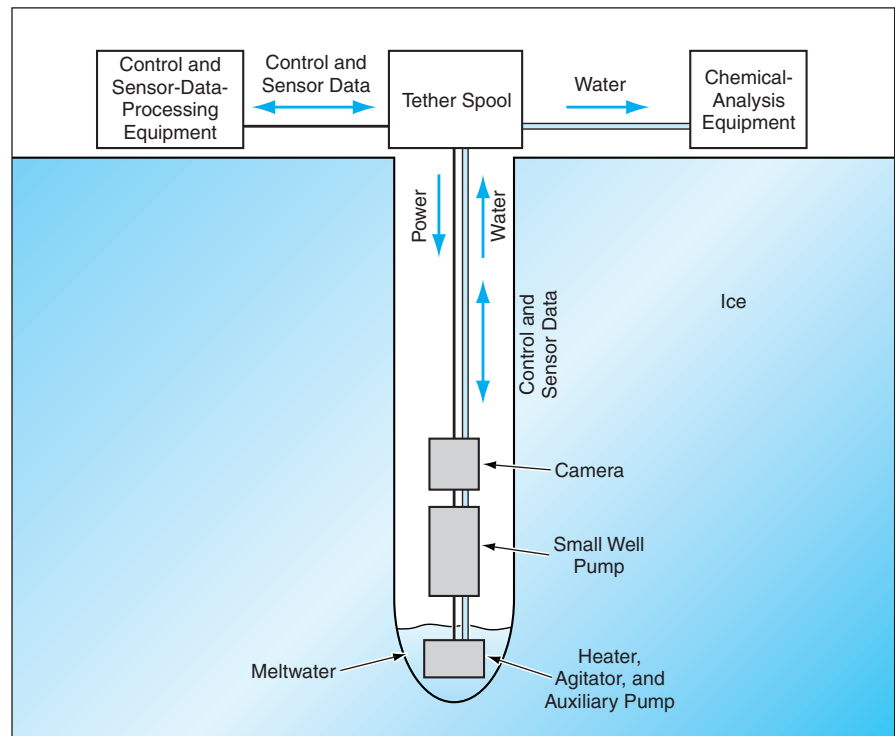
**Small samples of ice would be melted and pumped to the surface for analysis.**

*NASA's Jet Propulsion Laboratory, Pasadena, California*

The subsurface ice probe (SIPR) is a proposed apparatus that would bore into ice to depths as great as hundreds of meters by melting the ice and pumping the samples of meltwater to the surface. Originally intended for use in exploration of subsurface ice on Mars and other remote planets, the SIPR could also be used on Earth as an alternative to coring, drilling, and melting apparatuses heretofore used to sample Arctic and Antarctic ice sheets.

The SIPR would include an assembly of instrumentation and electronic control equipment at the surface, connected via a tether to a compact assembly of boring, sampling, and sensor equipment in the borehole (see figure). Placing as much equipment as possible at the surface would help to attain primary objectives of minimizing power consumption, sampling with high depth resolution, and unobstructed imaging of the borehole wall. To the degree to which these requirements would be satisfied, the SIPR would offer advantages over the aforementioned ice-probing systems.

The tether would include wires for power, wires or optical fibers for control and sensor data, and a narrow tube through which meltwater would be pumped to the surface. A unit containing a heater, a cam-driven agitator, and an auxiliary pump (a small peristaltic pump) would be submerged in a small pool of water at the bottom of the borehole. The heater in this unit would melt ice at the bottom of the hole. The agitator would prevent settling of any suspended sediment to the bottom of the hole. The auxiliary pump would quickly transfer the meltwater and any sediment to a small holding tank above the water surface. To minimize unwanted loss of energy through side melting and to optimize the depth resolution of



**Scientific Instruments and Control Equipment** would reside in an assembly at the surface. Only a small assembly of equipment essential for melting ice, pumping the meltwater, and inspecting the borehole wall would be lowered into the borehole.

meltwater samples, only a small amount of water would be left at the bottom of the hole.

The heart of the down-hole assembly would be a small well pump that would force the water and sediment from the holding tank, up through the tube, to the instrumentation assembly at the surface. The pump must provide sufficient head to lift the water from the greatest anticipated borehole depth. Alternatively, the down-hole assembly could be made smaller by placing a pump on the surface and using a two-way fluid or pneumatic loop to drive the liquid to the surface. The inevitable dissipation of electric energy in the power cables

could be utilized as auxiliary heating to prevent freezing of the water in the tube. Either above or below the pump there could be an electronic camera to acquire images of the borehole wall and/or a nephelometer for acquiring data on sediment particles trapped in the wall.

The design of the tube is anticipated to demand a major part of the overall design effort. The bore of the tube must be narrow enough that the mixing length within the tube corresponds to a short column of water in the hole: this length defines the depth resolution of the system (intended to be of the order of centimeters). At the same time, the

bore must not be so narrow that the consequent resistance to flow exceeds the capability of the well pump, and the bore must be wide enough to accommodate suspended particles. The tube

must not kink or fracture at low temperatures. It should be sufficiently insulated to prevent freezing during normal operation and it should tolerate inadvertent freezing.

*This work was done by Michael Hecht and Frank Carsey of Caltech for NASA's Jet Propulsion Laboratory. Further information is contained in a TSP (see page 1). NPO-40031*

## Real-Time Simulation of Aeroheating of the Hyper-X Airplane

Computational simulations are expected to provide guidance for initial design choices.

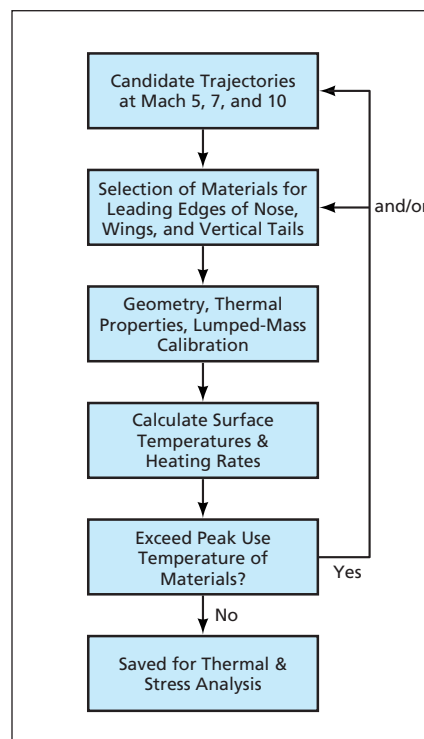
*Dryden Flight Research Center, Edwards, California*

A capability for real-time computational simulation of aeroheating has been developed in support of the Hyper-X program, which is directed toward demonstrating the feasibility of operating an air-breathing ramjet/scramjet engine at mach 5, mach 7, and mach 10. The simulation software will serve as a valuable design tool for initial trajectory studies in which aerodynamic heating is expected to exert a major influence in the design of the Hyper-X airplane; this tool will aid in the selection of materials, sizing of structural skin thicknesses, and selection of components of a thermal-protection system (TPS) for structures that must be insulated against aeroheating.

The Hyper-X airplane will include an inlet/combustor/nozzle assembly attached to an airframe. The forebody of the inlet will consist of a leading edge and a tungsten ballast. Movable wings and vertical tail rudders will give the autonomous airplane controllability. Mounted inside the airframe will be all the active systems needed to fly and to demonstrate the ramjet/scramjet engine. The fuel-burning and flight hardware will be instrumented to collect and telemeter flight data.

Because of the short duration of flight, critical areas on the airframe TPS will be limited to the leading edges on the nose, cowl, and side walls of the inlet and the horizontal wings and vertical

tails. In addition to other aeroheating effects, gap heating is expected to occur at horizontal wing roots, and at vertical rudder roots by amounts that will vary with movement of the rudders.



The **Computational Simulation of Aeroheating** is one of several real-time simulations used in initial design studies. This simulation can be used to eliminate flight trajectories that would give rise to local temperatures in excess of structural-design temperature limits.

The present capability for real-time computational simulation of aeroheating makes it possible to predict temperature as a function of time at critical heating locations on the Hyper-X airplane. Simulations of this type are used extensively to select acceptable flight trajectories by eliminating ones for which structural-design temperature limits would be exceeded (see figure). Other real-time simulations can be performed, using software modules that enable evaluation of other aspects of operation and design, including aerodynamics, reaction control system, flight guidance, and airplane structures. At speeds in excess of mach 2, aeroheating is considered important enough to affect design parameters, so that it becomes necessary to include a software module for simulation of aeroheating.

Thus far, a mathematical submodel of a nose with a solid carbon/carbon leading edge has been incorporated into the mathematical model used in the simulation of aeroheating. This submodel includes 14 temperature nodes. Other submodels of aeroheating of the tail rudder and the leading edges of the horizontal and vertical tails were undergoing development at the time of reporting the information for this article.

*This work was done by Les Gong of Dryden Flight Research Center. For further information, contact the Dryden Commercial Technology Office at (661) 276-3143. DRC-98-76*

## Using Laser-Induced Incandescence To Measure Soot in Exhaust

This system incorporates several improvements over prior LII soot-measuring systems.

*John H. Glenn Research Center, Cleveland, Ohio*

An instrumentation system exploits laser-induced incandescence (LII) to measure the concentration of soot particles in an exhaust stream from an en-

gine, furnace, or industrial process that burns hydrocarbon fuel. In comparison with LII soot-concentration-measuring systems that have been described in

prior *NASA Tech Briefs* articles, this system is more complex and more capable.

Like the other systems, this system includes a pulsed laser and associated op-

tics that shape and aim a laser beam through an exhaust stream. The laser beam heats entrained soot particles to incandescence. Light from the glowing soot particles is collected by two band-pass-filter-and-photodetector assemblies for measurement of the intensity of the incandescence as a function of time in two wavelength bands. On the basis of the established principle of two-color pyrometry, the instantaneous temperature of the glowing soot particles is determined from the ratio between the instantaneous intensities in the two wavelength bands.

The heating of the soot particles by absorption of laser light and the subsequent cooling of the particles through incandescence (and, when applicable, through evaporation of volatile materials from their surfaces) are complex nanoscale processes that can be represented by a computational model in which, during the decay of incandescence following the laser pulse, the time-dependent absolute intensities and the time-dependent temperature depend, further, on the volume concentration and surface area of the soot particles. In this system, the model is inverted

to obtain the number density and size of the primary soot particles. The mass density of soot averaged over the probe volume can then be calculated from the volume concentration.

Calibration of the photodetectors and the optical components that precede them is necessary for determining absolute intensities. In this system, calibration is performed by use of a strip-filament lamp or other extended light source that has a known radiance traceable to that of a standard source maintained by the National Institute of Standards and Technology.

Uniform heating of all soot particles in the probe volume and in a sheath volume surrounding the probe volume is necessary to ensure accuracy. To satisfy this requirement, (1) the laser beam is expanded into a sheet of finite thickness that is perpendicular to the viewing axis of the detecting optics, and (2) the detecting optics include an iris that defines the probe volume as a cylindrical central, mid-thickness region within the beam.

In prior LII systems, the laser fluence is so great that soot particles are heated to temperatures above the sublimation

temperature of carbon (about 4,000 K). This was done to produce an LII signal that was somewhat independent of laser fluence, making it unnecessary to measure the temperatures of soot particles. Unfortunately, the loss of mass through sublimation alters the very quantity (mass density of soot) that one seeks to measure. Also for prior LII systems, the laser fluence required to reach sublimation temperatures is dependent upon the initial particle temperature, and is affected by condensed species such as volatile organic compounds and water. In this self-calibrating system, the intensity measurements are used to adjust the laser fluence to keep the laser-heated soot particles below the sublimation temperature.

*This work was done by William D. Bachalo and Subramanian V. Sankar of Artium Technologies, Inc. for **Glenn Research Center**.*

*Inquiries concerning rights for the commercial use of this invention should be addressed to NASA Glenn Research Center, Commercial Technology Office, Attn: Steve Fedor, Mail Stop 4-8, 21000 Brookpark Road, Cleveland, Ohio 44135. Refer to LEW-17479-1.*

## Method of Real-Time Principal-Component Analysis

Hardware can be simplified.

NASA's Jet Propulsion Laboratory, Pasadena, California

Dominant-element-based gradient descent and dynamic initial learning rate (DOGEDYN) is a method of sequential principal-component analysis (PCA) that is well suited for such applications as data compression and extraction of features from sets of data. In comparison with a prior method of gradient-descent-based sequential PCA, this method offers a greater rate of learning convergence. Like the prior method, DOGEDYN can be implemented in software. However, the main advantage of DOGEDYN over the prior method lies in the facts that it requires less computation and can be implemented in simpler hardware. It should be possible to implement DOGEDYN in compact, low-power, very-large-scale integrated (VLSI) circuitry that could process data in real time.

For the purposes of DOGEDYN, the input data are represented as a succession of vectors measured at sampling times  $t$ . The objective function [the error measure (also called "energy" in the art) that one seeks to minimize in gradient-descent iterations] is defined by

$$J(w) = \sum_{i=1}^m J_i(w_i) = \sum_{i=1}^m \sum_{t=1}^k |x_t - w_i w_i^T x_t|$$

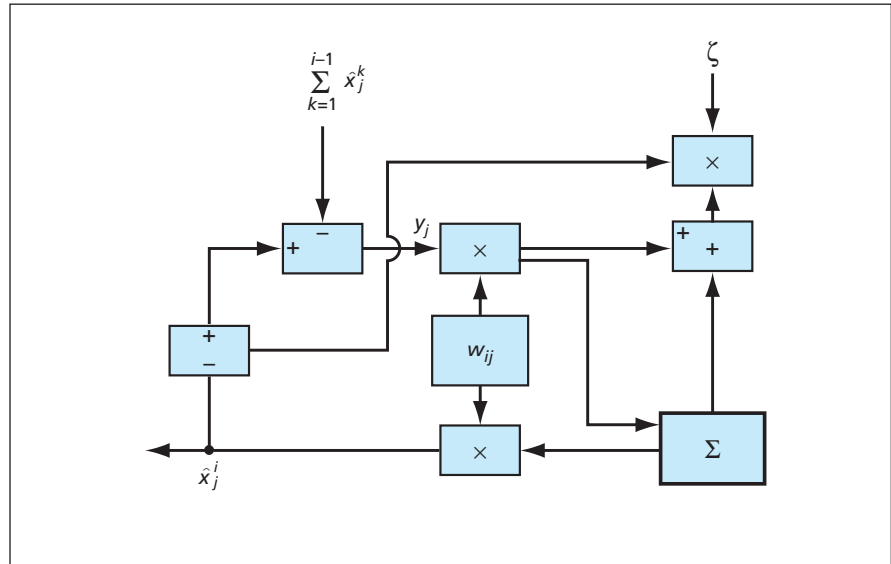
where  $m$  is the number of principal components,  $k$  is the number of sampling time intervals (the number of measurement vectors),  $x_t$  is the measured vector at time  $t$ , and  $w_i$  is the  $i$ th principal vector (equivalently, the  $i$ th eigenvector). The term  $J_i(w_i)$  in the above equation is further expanded by

$$J_i(w_i) = \sum_{t=1}^k |y_t - w_i w_i^T y_t|^2$$

and

$$y_t = x_t - \sum_{j=1}^{i-1} w_j w_j^T x_t$$

The learning algorithm in DOGEDYN involves sequential extraction of the



The Hardware Represented by This Diagram can be regarded as a unit that can be cascaded to obtain as many parallel eigenvector extractors as needed in a given application. The cascaded, identical units can be fabricated on a single integrated-circuit chip.

principal vectors by means of a gradient descent in which only the dominant element is used at each iteration. Omitting details of the mathematical derivation for the sake of brevity, an iteration includes updating of a weight matrix according to

$$W_{ij}^{\text{new}} = W_{ij}^{\text{old}} + \zeta \Delta w_{ij} = W_{ij}^{\text{old}} + \zeta \mathcal{E}_{ij} (w_i^T y_i + w_{ij} y_{ij})$$

where  $w_{ij}$  is an element of the weight matrix and  $\zeta$  is the dynamic initial learning rate, chosen to increase the rate of convergence by compensating for the energy lost through the previous extraction of principal components. The value of the dynamic learning rate is given by

$$\zeta = \frac{E_0}{E_{i-1}}$$

where  $E_0$  is the energy at the beginning of learning and  $E_{i-1}$  is the energy of the  $i-1$ st extracted principal component.

The figure depicts a hardware architecture for implementing DOGEDYN. The raw input data, here denoted  $x_j$ ,

are subtracted from the sum of the data previously projected on the previous principal components to obtain  $y_j$  (which is equivalent to  $y_t$  as defined above, after appropriate changes in subscripts). The  $\Sigma$  box calculates the inner product of vectors  $y$  and  $w_i$ . The output of the  $\Sigma$  box is summed with the previously computed product of  $y_j$  and  $w_{ij}$  and the result multiplied by the dynamic learning rate before updating of  $w_{ij}$ .

This work was done by Tuan Duong and Vu Duong of Caltech for NASA's Jet Propulsion Laboratory. Further information is contained in a TSP (see page 1).

In accordance with Public Law 96-517, the contractor has elected to retain title to this invention. Inquiries concerning rights for its commercial use should be addressed to:

Innovative Technology Assets Management  
JPL

Mail Stop 202-233

4800 Oak Grove Drive

Pasadena, CA 91109-8099

(818) 354-2240

E-mail: iaoffice@jpl.nasa.gov

Refer to NPO-40034, volume and number of this NASA Tech Briefs issue, and the page number.



# Σ Insect-Inspired Flight Control for Unmanned Aerial Vehicles

Relatively simple sensory and computing systems would generate remarkably effective control in flight to allow close-up approach to hard terrain.

NASA's Jet Propulsion Laboratory, Pasadena, California

Flight-control and navigation systems inspired by the structure and function of the visual system and brain of insects have been proposed for a class of developmental miniature robotic aircraft called "biomorphic flyers" described earlier in "Development of Biomorphonic Flyers" (NPO-30554), *NASA Tech Briefs*, Vol. 28, No. 11 (November 2004), page 54. These form a subset of biomorphonic explorers, which, as reported in several articles in past issues of *NASA Tech Briefs* ["Biomorphonic Explorers" (NPO-20142), Vol. 22, No. 9 (September 1998), page 71; "Bio-Inspired Engineering of Exploration Systems" (NPO-21142), Vol. 27, No. 5 (May 2003), page 54; and "Cooperative Lander-Surface/Aerial Microflyer Missions for Mars Exploration" (NPO-30286), Vol. 28, No. 5 (May 2004), page 36], are proposed small robots, equipped with microsensors and com-

munication systems, that would incorporate crucial functions of mobility, adaptability, and even cooperative behavior. These functions are inherent to biological organisms but are challenging frontiers for technical systems. Biomorphonic flyers could be used on Earth or remote planets to explore otherwise difficult or impossible to reach sites. An example of an exploratory task of search/surveillance functions currently being tested is to obtain high-resolution aerial imagery, using a variety of miniaturized electronic cameras.

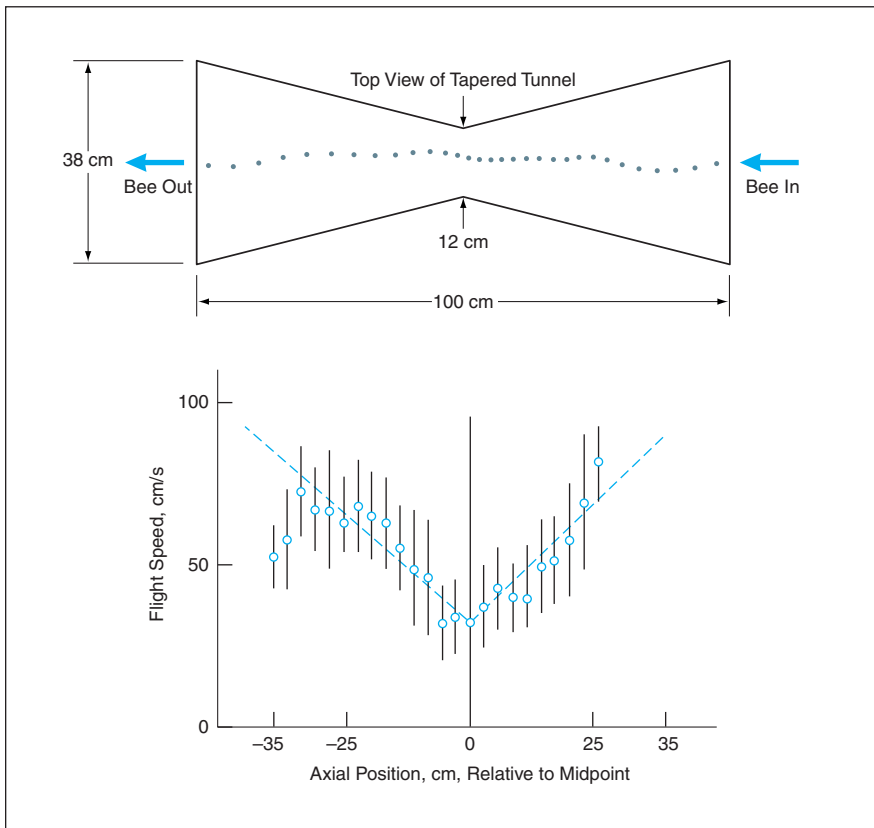
The control functions to be implemented by the systems in development include holding altitude, avoiding hazards, following terrain, navigation by reference to recognizable terrain features, stabilization of flight, and smooth landing. Flying insects perform these and other functions remarkably well, even

though insect brains contains fewer than  $10^{-4}$  as many neurons as does the human brain. Although most insects have immobile, fixed-focus eyes and lack stereoscopy (and hence cannot perceive depth directly), they utilize a number of ingenious strategies for perceiving, and navigating in, three dimensions. Despite their lack of stereoscopy, insects infer distances to potential obstacles and other objects from image motion cues that result from their own motions in the environment. The concept of motion of texture in images as a source of motion cues is denoted generally as the concept of optic or optical flow. Computationally, a strategy based on optical flow is simpler than is stereoscopy for avoiding hazards and following terrain. Hence, this strategy offers the potential to design vision-based control computing subsystems that would be more compact, would weigh less, and would demand less power than would subsystems of equivalent capability based on a conventional stereoscopic approach.

These control loops for stabilizing attitude and/or holding altitude would include optoelectronic ocelli and would be based partly on dragonfly ocelli—simple eyes that exist in addition to the better-known compound eyes of insects. In many insects the ocelli only detect changes in light intensity and have minimal observable effect on flight. In dragonflies, the ocelli play an important role in stabilizing attitude with respect to dorsal light levels. The control loops to be implemented would incorporate elements of both dragonfly ocellar functions and optical flow computation as derived from principles observed in honeybee flight.

On Earth, bees use sky polarization patterns in the ultraviolet part of the spectrum as a direction reference relative to the position of the Sun. A robotic direction-finding technique based on this concept is more robust in comparison with a simple Sun compass because the ultraviolet polarization pattern is distributed across the entire sky on Earth and is redundant and hence can be extrapolated from a small region of clear sky in an elsewhere cloudy sky that hides the Sun.

A bee tends to adjust its flight speed to maintain a constant optical flow (that is,



**Bees Flew Through a Tapered Tunnel** in an experiment on how they use visual cues to control flight. The bees decelerated as the tunnel narrowed, then accelerated as it widened. The dashed line shows the flight-speed profile that one would obtain if the bees were to hold the angular velocity of the images of the walls constant at  $320^\circ$  per second. An obvious advantage of regulating flight speed to obtain constant image speed is that an insect would automatically decelerate to a safer speed to negotiate a narrow passage.

a constant angular velocity of the image of the environment) over its compound eye (see figure). Consistent with this strategy, a bee utilizes the following simple control laws when approaching a landing site on a flat surface:

1. The optical flow of the surface is held constant throughout the descent.
2. Forward speed is held proportional to vertical speed throughout the descent.

This simple combination of control laws enables a smooth landing with minimal computation. The forward speed and rate of descent are reduced together, and are both close to zero at touchdown. No knowledge or measurement of instantaneous speed or height above the ground are necessary. This combination of control laws can readily be modified for a biomorphic flyer,

which has a nonzero stalling speed.

*This work was done by Sarita Thakoor of Caltech for NASA's Jet Propulsion Laboratory and by G. Stange, M. Srinivasan, and Javaan Chahl of Australian National University and Butler Hine and Steven Zornetzer of Ames Research Center for the NASA Intelligent Systems Program. Further information is contained in a TSP (see page 1). NPO-30545*

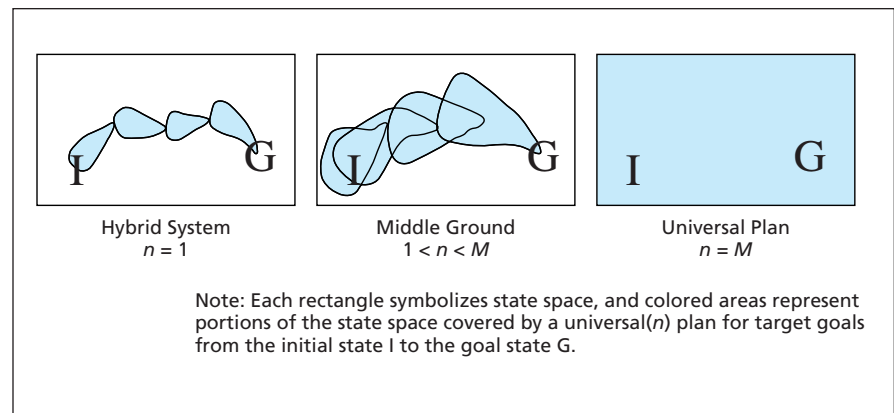
## Domain Compilation for Embedded Real-Time Planning

**Robustness is increased at the price of a moderate increase in complexity.**

*NASA's Jet Propulsion Laboratory, Pasadena, California*

A recently conceived approach to automated real-time control of the actions of a robotic system enables an embedded real-time planning algorithm to develop plans that are more robust than they would otherwise be, without imposing an excessive computational burden. This approach occupies a middle ground between two prior approaches known in the art as the universal-plan and hybrid approaches.

Ever since discovering the performance limitations of taking a sense-plan-act approach to controlling robots, the robotics community has endeavored to follow a behavior-based approach in which a behavior includes a rapid feedback loop between state estimation and motor control. Heretofore, system architectures following this approach have been based, variously, on algorithms that implement universal plans or algorithms that function as hybrids of planners and executives. In a typical universal-plan case, a set of behaviors is merged into the plan, but the system must be restricted to relatively small problem domains to avoid having to reason about too many states and represent them in the plan. In the hybrid approach, one implements actions as small sets of behaviors, each applicable to a limited set of circumstances. Each action is intended to bring the system to a subgoal state. A planning algorithm is used to string these actions together into a sequence to traverse the state space from an initial or current state to a goal state. The hybrid approach works well in a static environment, but it is inherently brittle in a dynamic environment because a failure can occur when the environment strays beyond the region of applicability of the current activity.



Coverage of State Space by an  $n$ -level plan increases with  $n$ .

In the present approach, a system can vary from the hybrid approach to the universal-plan approach, depending on a single integer parameter, denoted  $n$ , which can range from 1 to a maximum domain-dependent value of  $M$ . As illustrated in the figure,  $n = 1$  represents the hybrid approach, in which each linked action covers a small part of the state space of the system. As  $n$  increases, the portion of state space associated with each action and its subgoal grows. When  $n$  reaches  $M$ , coverage extends over the full state space, so that the system contains a universal plan.

Through incorporation of an embedded real-time planning algorithm that follows this middle-ground approach, a hybrid system can be made much more robust in a dynamic environment. In such a system, the planning algorithm passes the current subgoals (instead of activities) to an executive algorithm. The executive algorithm then uses the real-time planning algorithm to determine when to perform which action until it determines either that the current subgoals have been reached or that

they cannot be reached within  $n$  steps. If the current subgoals have been reached, the planning algorithm gives new subgoals to the executive algorithm. If it has been determined that the current subgoals cannot be reached, the planning algorithm must alter the sequence of actions.

A structure for finding the next step on an  $n$  or fewer step path to a subgoal is called a universal( $n$ ) plan. Because complexity increases sharply with  $n$ , it is necessary to choose  $n$  small enough to avoid an excessive computational burden but large enough that it is possible to make a universal( $n$ ) plan that makes the system robust in the sense that it can reach each given subgoal state from any state in a large region of the state space.

This approach involves utilizing knowledge compilation research by implementing an off-line compiler that generates a universal( $n$ ) plan from a system description. In the first step of a two-step process, the system description is converted into a logical expression, in what is known as a conjunctive nor-

mal form (CNF) that is based on the effects and preconditions of actions in an  $n$ -step plan. In the second step, the aforementioned research results are used to convert the CNF representation into a decomposable negation normal form (DNNF) representation. It turns

out that the computation time needed to evaluate a DNNF expression to compute an optimal  $n$ -step plan increases only linearly with the DNNF representation size.

*This work was done by Anthony Barrett of Caltech for NASA's Jet Propulsion Labo-*

*ratory. Further information is contained in a TSP (see page 1).*

*The software used in this innovation is available for commercial licensing. Please contact Don Hart of the California Institute of Technology at (818) 393-3425. Refer to NPO-40296.*

## Σ Semantic Metrics for Analysis of Software

**These metrics represent a more human-oriented view of software.**

*Goddard Space Flight Center, Greenbelt, Maryland*

A recently conceived suite of object-oriented software metrics focus is on semantic aspects of software, in contradistinction to traditional software metrics, which focus on syntactic aspects of software. Semantic metrics represent a more human-oriented view of software than do syntactic metrics. The semantic metrics of a given computer program are calculated by use of the output of a knowledge-based analysis of the program, and are substantially more representative of software quality and more readily comprehensible from a human perspective than are the syntactic metrics.

Semantic metrics have the potential to help software engineers identify fragile, low-quality sections of code much earlier in the development process than is possible by use of syntactic metrics. By enabling earlier and better detection of faults, semantic metrics are expected to make maintenance of software less time-consuming and

expensive and to make software more reusable. Because it is less costly to correct faults found earlier than to correct faults found later in the software-development process, it is expected that the overall cost of developing software will be reduced. Moreover, because semantic metrics provide better measures of internal documentation descriptiveness (descriptiveness of the comments and identifiers in software), all aspects of development of software can be expected to benefit from improved understanding of the software.

Prototype software called "SemMet" for computing semantic metrics is undergoing development. In SemMet, semantic metrics are described within the context of knowledge-based systems that consist of semantic networks formed from conceptual graphs. Conceptual graphs are often used for semantic networks for natural language processing; however, the use of conceptual graphs is also a general and fairly common

knowledge-representation technique. In the computation of semantic metrics, concepts and conceptual relations from conceptual graphs inside a knowledge base are used as input. The output semantic metrics are presented in a report.

*This work was done by Letha H. Etkorn, Glenn W. Cox, Phil Farrington, Dawn R. Utley, Sampson Ghalston, and Cara Stein of the University of Alabama at Huntsville for Goddard Space Flight Center. Further information is contained in a TSP (see page 1).*

*In accordance with Public Law 96-517, the contractor has elected to retain title to this invention. Inquiries concerning rights for its commercial use should be addressed to:*

*Letha Hughes Etkorn, Ph.D., P.E.*

*Assistant Professor*

*Computer Science Department*

*University of Alabama in Huntsville*

*Huntsville, AL 35899*

*Refer to GSC-14752-1, volume and number of this NASA Tech Briefs issue, and the page number.*

## Σ Simulation of Laser Cooling and Trapping in Engineering Applications

**This design instrument shows good agreement with experimental measurements.**

*NASA's Jet Propulsion Laboratory, Pasadena, California*

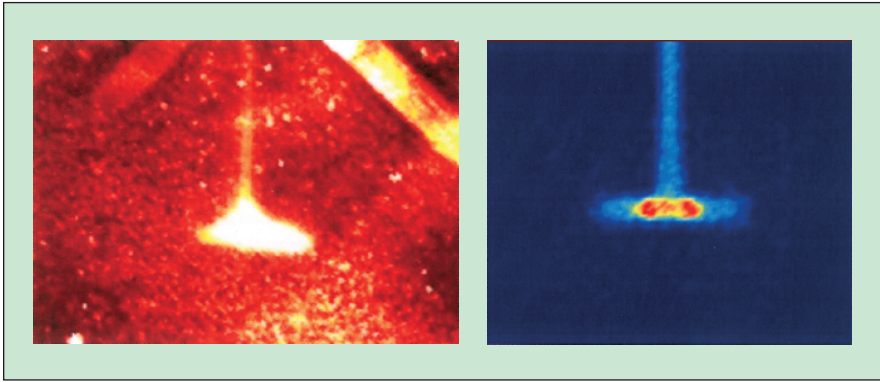
An advanced computer code is undergoing development for numerically simulating laser cooling and trapping of large numbers of atoms. The code is expected to be useful in practical engineering applications and to contribute to understanding of the roles that light, atomic collisions, background pressure, and numbers of particles play in experiments using laser-cooled and -trapped atoms. The code is based on semiclassical theories of the forces exerted on atoms by magnetic and optical fields.

Whereas computer codes developed previously for the same purpose account for only a few physical mechanisms, this code incorporates many more physical mechanisms (including atomic collisions, sub-Doppler cooling mechanisms, Stark and Zeeman energy shifts, gravitation, and evanescent-wave phenomena) that affect laser-matter interactions and the cooling of atoms to submillikelvin temperatures. Moreover, whereas the prior codes can simulate the interactions of at most a few atoms with a reso-

nant light field, the number of atoms that can be included in a simulation by the present code is limited only by computer memory. Hence, the present code represents more nearly completely the complex physics involved when using laser-cooled and -trapped atoms in engineering applications.

Another advantage that the code incorporates is the possibility to analyze the interaction between cold atoms of different atomic number. Some properties that cold atoms of different atomic





A **Cold Atomic Beam** is shown emerging from a magneto-optical trap in a pyramidal-low-velocity-intense-source configuration. The figure shows a comparison between experiment (left) and simulation (right). The images depict an area of approximately  $1.5 \times 1.5$  cm.

species have, like cross sections and the particular excited states they can occupy when interacting with each other and light fields, play important roles not yet completely understood in the new experiments that are under way in laboratories worldwide to form ultracold molecules. Other research efforts use cold atoms as holders of quantum information, and more recent developments in cavity quantum electrodynamics also use ultracold atoms to explore and expand new information-technology ideas. These experiments give a hint on

the wide range of applications and technology developments that can be tackled using cold atoms and light fields. From more precise atomic clocks and gravity sensors to the development of quantum computers, there will be a need to completely understand the whole ensemble of physical mechanisms that play a role in the development of such technologies.

The code also permits the study of the dynamic and steady-state operations of technologies that use cold atoms. The physical characteristics of lasers

and fields can be time-controlled to give a realistic simulation of the processes involved such that the design process can determine the best control features to use.

It is expected that with the features incorporated into the code it will become a tool for the useful application of ultracold atoms in engineering applications. Currently, the software is being used for the analysis and understanding of simple experiments using cold atoms, and for the design of a modular compact source of cold atoms to be used in future research and development projects. The results so far indicate that the code is a useful design instrument that shows good agreement with experimental measurements (see figure), and a Windows-based user-friendly interface is also under development.

*This program was written by Jaime Ramirez-Serrano, James Kohel, Robert Thompson, Nan Yu, and Nathan Lunblad of Caltech for NASA's Jet Propulsion Laboratory. Further information is contained in a TSP (see page 1).*

*This software is available for commercial licensing. Please contact Don Hart of the California Institute of Technology at (818) 393-3425. Refer to NPO-30595.*





### **Large Fluvial Fans and Exploration for Hydrocarbons**

A report discusses the geological phenomena known, variously, as modern large (or large modern) fluvial fans or large continental fans, from a perspective of exploring for hydrocarbons. These fans are partial cones of river sediment that spread out to radii of 100 km or more. Heretofore, they have not been much recognized in the geological literature — probably because they are difficult to see from the ground. They can, however, be seen in photographs taken by astronauts and on other remotely sensed imagery. Among the topics discussed in the report is the need for research to understand what seems to be an association among fluvial fans, alluvial fans, and hydrocarbon deposits. Included in the report is an abstract that summarizes the global distribution of large modern fluvial fans and a proposal to use that distribution as a guide to understanding paleo-fluvial reservoir systems where oil and gas have formed. Also included is an abstract that summarizes what a continuing mapping project has thus far revealed about the characteristics of large fans that have been found in a variety of geological environments.

*This work was done by Murray Justin Wilkinson of Lockheed Martin Corp. for Johnson Space Center.*

*This invention is owned by NASA, and a patent application has been filed. Inquiries concerning nonexclusive or exclusive license for its commercial development should be addressed to the Patent Counsel, Johnson Space Center, (281) 483-0837. Refer to MSC-23424.*

### **Doping-Induced Interband Gain in InAs/AlSb Quantum Wells**

A paper describes a computational study of effects of doping in a quantum well (QW) comprising a 10-nm-thick layer of InAs sandwiched between two 21-nm-thick AlSb layers. Heretofore, InAs/AlSb QWs have not been useful as interband gain devices because they have type-II energy-band-edge alignment, which causes spatial separation of

electrons and holes, thereby leading to weak interband dipole matrix elements. In the doping schemes studied, an interior sublayer of each AlSb layer was doped at various total areal densities up to  $5 \times 10^{12} \text{ cm}^{-2}$ . It was found that (1) proper doping converts the InAs layer from a barrier to a well for holes, thereby converting the heterostructure from type II to type I; (2) the resultant dipole matrix elements and interband gains are comparable to those of typical type-I heterostructures; and (3) dipole moments and optical gain increase with the doping level. Optical gains in the transverse magnetic mode can be almost ten times those of other semiconductor material systems in devices used to generate medium-wavelength infrared (MWIR) radiation. Hence, doped InAs/AlSb QWs could be the basis of an alternative material system for devices to generate MWIR radiation.

*This work was done by K. I. Kolokolov and C. Z. Ning of Ames Research Center. Further information is contained in a TSP (see page 1).*

*Inquiries concerning rights for the commercial use of this invention should be addressed to the Patent Counsel, Ames Research Center, (650) 604-5104. Refer to ARC-15157-1*

### **Development of Software for a Lidar-Altitude Processor**

A report describes the development of software for a digital processor that operates in conjunction with a finite-impulse-response (FIR) chip in a spaceborne lidar altimeter. Processing is started by a laser-fire interrupt signal that is repeated at intervals of 25 ms. For the purpose of discriminating between returns from the ground and returns from such things as trees, buildings, and clouds, the software is required to scan digitized lidar-return data in reverse of the acquisition sequence in order to distinguish the last return pulse from within a commanded ground-return range window. The digitized waveform information within this range window is filtered through 6 matched filters, in the hardware electronics, in order to maximize the probability of finding echoes from sloped or rough terrain and minimize the probability of selecting cloud returns. From

the data falling past the end of the range window, there is obtained a noise baseline that is used to calculate a threshold value for each filter. The data from each filter is analyzed by a complex weighting scheme and the filter with the greatest weight is selected. A region around the peak of the ground-return pulse associated with the selected filter is placed in telemetry, as well as information on its location, height, and other characteristics. The software requires many uplinked parameters as input. Included in the report is a discussion of major software-development problems posed by the design of the FIR chip and the need for the software to complete its process within 20 ms to fit within the overall 25-ms cycle.

*This work was done by Jacob S. Rosenberg and Carlos Trujillo of Goddard Space Flight Center. Further information is contained in a TSP (see page 1). GSC-14382*

### **Upgrading the Space Shuttle Caution and Warning System**

A report describes the history and the continuing evolution of an avionic system aboard the space shuttle, denoted the caution and warning system, that generates visual and auditory displays to alert astronauts to malfunctions. The report focuses mainly on planned human-factors-oriented upgrades of an alphanumeric fault-summary display generated by the system. Such upgrades are needed because the display often becomes cluttered with extraneous messages that contribute to the difficulty of diagnosing malfunctions. In the first of two planned upgrades, the fault-summary display will be rebuilt with a more logical task-oriented graphical layout and multiple text fields for malfunction messages. In the second upgrade, information displayed will be changed, such that text fields will indicate only the sources (that is, root causes) of malfunctions; messages that are not operationally useful will no longer appear on the displays. These and other aspects of the upgrades are based on extensive collaboration among astronauts, engineers, and human-factors scientists. The report describes the human-factors principles applied in the upgrades.

*This report was written by Jeffrey W. McCandless and Robert S. McCann of Ames Research Center and Bruce R. Hilty of Johnson Space Center. Further information is contained in a TSP (see page 1).  
ARC-15178-1*



### **Fractal Reference Signals in Pulse-Width Modulation**

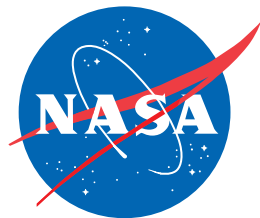
A report proposes the use of waveforms having fractal shapes reminiscent of sawteeth (in contradistinction to conventional regular sawtooth waveforms) as ref-

erence signals for pulse-width modulation in control systems for thrusters of spacecraft flying in formation. Fractal reference signals may also be attractive in some terrestrial control systems — especially those in which pulse-width modulation is used for precise control of electric motors. The report asserts that the use of fractal reference signals would enable the synchronous control of several variables of a spacecraft formation, such that consumption of propellant would be minimized, intervals between thruster firings would be long (as preferred for performing scientific observations), and delays in con-

trolling large-thrust maneuvers for retargeting would be minimized. The report further asserts that whereas different controllers would be needed for different modes of operation if conventional pulse-width modulation were used, the use of fractal reference signals would enable the same controller to function nearly optimally in all regimes of operation, so that only this one controller would be needed.

*This work was done by Boris Lurie of Caltech and Helen Lurie of UCLA for NASA's Jet Propulsion Laboratory. Further information is contained in a TSP (see page 1).  
NPO-30402*





National Aeronautics and  
Space Administration